

國立臺灣大學電機資訊學院電信工程學研究所

博士論文

Graduate Institute of Communication Engineering
College of Electrical Engineering and Computer Science
National Taiwan University



Doctoral Dissertation

具有強健性之非線性特徵提取法應用於臨床醫學
Robust Methods for Nonlinear Behavior Identification in
Clinical Applications

張儀中

Yi-Chung Chang

指導教授：曹建和 博士

Advisor : Jenho Tsao, Ph.D.

中華民國 104 年 1 月

Jan, 2015

致 謝

念博班對我而言向來不是意料中的事，自從碩班受到曹老師啟發，接觸了醫用超音波領域，也跟著高中同學楊智傑，與尹彙文與許淑霞醫師接觸了心率變異相關領域，畢業後因緣際會地從較擅長的電子產業做到挑戰性高的醫療儀器領域，一路走來跌跌撞撞，過程中也慢慢了解到自己在醫療領域的不足之處，因而決定攻讀博士。

在念博班的過程中，因為興趣所以研究越做越深，卻往往難以收斂，多虧了我的學長羅孟宗老師，亦師亦友的指導兼鼓勵，還有一起研究努力的多個團隊，包括了東華的吳賢財老師與其實驗室成員，台大何亦倫主任與林彥宏醫師、黃惠君醫師，林亮宇醫師與葉惠敏醫師，北榮陳適安主任與林彥璋醫師、鍾法博醫師，國泰王拔群主任與其團隊，終能將這些過程轉換成具體研究。

研究中所用到的許多方法也都仰賴中央大學數據中心黃鏐主任與彭仲康教授的指導，還有中心許多同事於論文上的協助包括王淵弘博士、王政嚴博士、楊緒文博士、葉家榮博士、林澂博士。特別感謝林澂在許多方面尤其是生理上的意見，給了我很多啟發，還有感謝所有中心的研究助理，在許多研究上都幫忙了不少忙，還有中心的行政助理們，有你們的默默支持，讓許多研究能順利進行。

最後，將本篇論文獻給我的家人，沒有你們的支持就沒有現在的成果。

張儀中 於民國 104 年 1 月

Contents



中文摘要	5
Abstract	6
1 Introduction	8
1.1 Homeostasis and Correlations	8
1.2 Heart Rate Variability and Autonomic Nervous System	9
1.3 Dynamical System and Orbits	10
1.4 Reconstruct the Dynamics	12
1.5 Multiple Time Scale Dynamics	14
1.6 Attracting Orbit and Discrete Dynamical System	16
2 Quantization of Multi-scale correlation	21
2.1 Application of a Modified Entropy Computational Method in Assessing the Complexity of Pulse Wave Velocity Signals in Healthy and Diabetic Subjects	21
2.2 Outlier-resilient complexity analysis of heart beat dynamics ...	33
3 Quantification of Attracting Orbit	48
3.1 New Method to Noninvasively Monitor Fetal Heart Rate during Cesarean Section	48
3.2 Nonlinear Analysis of Fibrillatory Electrogram Similarity to Optimize the Detection of Complex Fractionated Electrograms During Persistent Atrial Fibrillation	63
4 Conclusion	81

中文摘要

近年來，許多領域持續發現及探討身體系統的複雜性，透過分子生物與病理機轉的研究，這些複雜機轉最終很可能會形成一個完整理論。另一方面，生醫信號分析也從生理系統的複雜性與調控理論之中發展出一些方法，能提取複雜特質和數據之下的訊息。這些非線性特徵提取方法，能夠從模糊不清的訊息下找出非線性的特徵作為疾病的判斷依據，其中一些方式也被證實效果優於傳統方法。然而非線性特徵卻容易受到臨床條件和環境的限制，如有限的數據長度，資料偶有會有參差不齊或是雜訊干擾。除此之外，提取方法也會造成失真，所使用之方法也可能無法有效濾除其他因素影響，有時甚至會大大增加後續分析的困難。本研究提出數種強健性的改良方法用來識別臨床數據的非線性特徵，以滿足臨床要求。

第一個探討的非線性特徵是訊息在多尺度的相關性，衡量方式是用資訊理論中的熵及渾沌碎形理論中的尺度，以不同時間尺度下的相關性，衡量系統的複雜特質。其中一個應用是透過計算血管動脈脈搏波速資訊的多尺度相關性，於大尺度的計算中增加計算準確度的方法，病患的量測時間能大幅減少到 12 分鐘。本方法能以較小的樣本大小(即 600 個連續信號)，在區分健康、中年、糖尿病患之間，達到與傳統的方法(即 1000 個連續信號)同樣的靈敏度。

另一個應用是在心率變異度分析中多尺度相關性的計算，透過改良的方法來抵抗心律不整因素的干擾，用於辨別安裝葉克膜病患的存活率。這項研究中提出了一種新的方法，通過分析在不同時間尺度的符號時間序列的不規則性來估計信號的複雜性，能有效避免葉克膜病患頻繁發生的心律不整所造成的干擾，該方法能夠檢測心臟調節功能的降低，並避免治療充血性心臟衰竭和葉克膜重症患者更加惡化。研究結果顯示，在嚴重干擾又同時有大量異常數值的心跳序列中，本方法能夠可靠地評估其多尺度的複雜性，因此可以作為一個有效的臨床工具，用於監控重症患者的心率調節功能。

第二個探討的非線性特徵是動態系統軌道的特質，這是透過相位空間軌跡計算而得。其中一個應用是在剖腹分娩過程中，以非侵方式從母體腹部體表取得心電圖，再透過幾種強健方法的處理，得出胎兒心電圖。最後透過類週期特性將胎兒心跳辨識出來，並使用心率變異參數量化軌跡，以獲取剖腹產對胎兒心跳與神經系統的作用。這項研究結果顯示，麻醉前，麻醉後，和分娩前 5 分鐘心率變異都明顯上升，該方法能夠可靠地評估胎兒對手術的反應，未來可以作為一個臨床工具，用於監控剖腹分娩過程中胎兒的狀態。

另一個應用是利用非線性波形相似度分析方法用於心房電圖，以找出重要的複雜碎裂心房電圖區域供心房電燒手術之用。該方法首先利用軌道的特徵找出每段週期，然後計算相空間這些軌跡的統計特性(相似性指數)。研究結果顯示，相似性指數在電燒成功病患的複雜碎裂心房電圖區域上較高，此類病患的預後也較好，這暗示了複雜碎裂心房電圖區域中相似性指數高的部分跟心房振顫的產生與維持有關聯。

Abstract

In recent years, the complexity of human body has been continuously revealed and discussed in many fields, it may eventually lead to a complete theory through the studies on pathogenesis and molecular biology of disease. On the other hand, the complex theory combined with the homeostasis mechanism has been used for biomedical signal analysis trying to identify such complex phenomena and underlying information behind the clinic data. These methods can help to extract non-linear feature from ambiguous information as the disease assessments, some of them have been accepted to have more advantages than traditional ones. However, such refining procedure are subject to many restrictions in clinical conditions and environments, such as limited data length, information may be occasional uneven or noise interfered. In addition, the extraction itself can also lead to distortions, the interference from other mechanism may not be effectively removed which raised the difficulty on the subsequent analysis. Therefore, this thesis proposes several robust methods to identify the specific nonlinear features in clinic data series and try to fulfill the clinical requirements.

The first portion of nonlinear feature is quantization of multi-scale correlation. It was derived from the entropy in information theory as well as the coarse-graining in chaos-fractal theory to quantify the complexity of a system through the correlations at different time scale. In the first study, a novel approach has been proposed to decrease the length of data in complexity calculation of pulse wave velocity (PWV) such that the time for data acquisition can be substantially reduced to 12 minutes. It utilized a smaller sample size (i.e. 600 consecutive signals) with remarkable preservation of sensitivity in differentiating among the healthy, aged, and diabetic populations compared with the conventional method (i.e. 1000 consecutive signals).

The second study utilized the multi-scale correlation of heart beat intervals (RRI) on critical patients whose life continuation relies on extracorporeal membrane oxygenator (ECMO). This study propose a new approach to estimate the complexity in a signal by analyzing the irregularity of the sign time series of coarse-grained time series at different time scales. Without removing any outliers due to ectopic beats, the method is able to detect a degradation of cardiac control in patients with congestive heart failure and a more degradation. Moreover, the derived complexity measures can predict the

mortality of ECMO patients. These results indicate that the proposed method may serve as a promising tool for monitoring cardiac function of patients in clinical settings.

In the second portion of nonlinear feature, the trajectories on phase space have been used for calculating statistical properties of the orbits in a dynamic system. In the first study, a novel method been proposed to noninvasively derive the fetus ECG signals from the maternal abdominal ECG during the cesarean section (CS). The heart beat series derived from the noisy signal were then quantified by several heart rate variability (HRV) methods. Moat parameters tell that the HRV increased 5 minutes after anesthesia and 5 minutes before delivery. These results shows that the proposed method may serve as a promising tool to obtain significant information about the fetal condition during labor.

In the second study, a nonlinear-based waveform similarity analysis of the local electrograms has been proposed, aiming to detect crucial complex fractionated atrial electrograms (CFEs) in atrial fibrillation (AF) ablation. This method firstly identify each cycle of orbits in the dynamic system and then calculate the statistical properties (similarity index, SI) of these trajectories on phase space. The result shows the average SI of the targeted CFEs was higher in termination patients, and they had a better outcome. This study suggested that sites with a high level of fibrillation electrogram similarity at the CFE sites were important for AF maintenance.



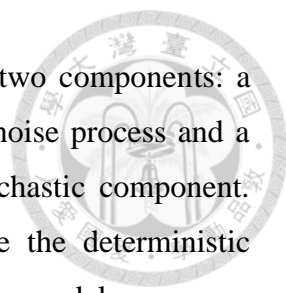
Chapter 1 Introduction

1.1 Homeostasis and Correlations

Living creatures can accept environmental stimulus, generate the appropriate responses, and automatically keep the cells, tissues and organs maintained in an optimal state that allow them to adjust its performance to the varying internal and external demands. In the short term, the mechanisms in human body involved the control of cardiac and respiratory rate, blood glucose concentration and body temperature. In the long term, the control of circadian rhythms, regulation of inflammatory processes and control of the immune system were also involved. As a result, our body contains different control loops to stay alive and this phenomenon is called "homeostasis" which is vital to life and important for disease assessment [1, 2].

All homeostatic control mechanisms have three main components for regulation: a receptor that monitors and responds to environmental changes. A control center that determines an appropriate response to the stimulus. A effector that can receive signals from the control center [3]. Through these components and pathways, a change will occur on the effector to correct the deviation by depressing it with negative feedback [2, 4]. When the stimulus occurred and followed by a change on the effector, a time-lagged causal relation between them has been built. The states of the control system may be represented by a time series so that data in the series will fluctuates between the stimulus and response. The time-lagged correlations might arise in such time series. Conceptually, the time-lagged correlations existing in a physiological data series implies regulation in the homeostatic system, the time scale can range from several milliseconds (e.g. for neurons) to several days (e.g. for immune system response to vaccination) [4- 6].

Based on causality and feedback, the early studies on homeostasis model is almost equivalent to that on the regulatory system, i.e., the control theory. Although the application of traditional control theory helps people to predict the behavior of simple systems in the body, the handling of a complex system such as immunologic network is difficult and sometimes does not lead to satisfactory solutions [6]. As a result, based on the time-lagged correlate properties, some studies try to apply the autoregressive (AR) to model the homeostatic process and estimate the system response. The AR modeling



assume that any stationary process can be expressed as a sum of two components: a stochastic component that a linear combination of lags of a white noise process and a deterministic component which is uncorrelated with the latter stochastic component. The noise source is reminiscent of the external stimulates while the deterministic component is reminiscent of the set-points. By applying this model, one can mathematically estimations the response of a system through the multiple realizations [7].

However, stationary model still relies on the assumptions of simple stationary process which may not be able to provide a comprehensive view for disorders or diseases. Under normal healthy conditions, the physiological fluctuations are usually neither random nor too regular that system is under control and behaves stationary. On the contrary, when multiple factors interact to produce the imbalance, particularly under serious disease, the physiological fluctuations may become unpredictable [8]. The system is out of control and becomes non-stationary, there is no numerical solution in such condition. As a result, it would be preferable to identify system states from correlations rather than solve the underlying equations in clinical applications.

1.2 Heart Rate Variability and Autonomic Nervous System

As mentioned earlier, homeostatic regulations in human body involved the control of cardiac rate [3], therefore, quantifying the physiological fluctuations through the easily accessible heart beat series has becomes popular in recent years [9-11]. The fluctuations on cardiac rate is measured through the variation in the beat-to-beat intervals and represented by the heart rate variability (HRV). The heart beats are originally trigger by the sinoatrial node (SA node) such that most variations are the results from different inputs of SA node. The main inputs are the autonomic nervous system and humoral factors. Other inputs includes the respiratory arrhythmia and the low-frequency oscillations associated with Mayer waves of blood pressure [12].

The electrical impulse from SA node may be delayed or blocked on an unhealthy heart tissues that leads to irregular heart beat and causes errors in the calculation of the HRV [13]. Therefore, traditional HRV analysis only calculate the normal sinus rhythms, i.e. N-N intervals, such as SDNN (standard deviation of NN intervals), pNN50 (proportion of successive NNs that differ by more than 50ms), power spectral bands of

the interpolated NN intervals. The high frequency (HF) band ranges from 0.15 to 0.4 Hz, low frequency (LF) ranges from 0.04 to 0.15 Hz, and the very low frequency (VLF) ranges from 0.0033 to 0.04 Hz [14].

Although cardiac automaticity is intrinsic to SA node, heart rate and rhythm are largely under the control of autonomic nervous system (ANS). The ANS is responsible for maintaining homeostasis and regulates the function of all innervated tissues and organs throughout the vertebrate body [15]. Since homeostatic regulation are important and required for survival, the actions of the ANS usually occur independent of our consciousness as the name suggests. The ANS has two divisions that work to counteract each other and keep the body in balance, the sympathetic nervous system (SNS) and the parasympathetic nervous system (PSNS). Decreased PSNS activity or increased SNS activity will result in reduced HRV. And the high frequency activity has been linked to PSNS activity [16].

Typically, reduction of HRV is associated with ill state, and such symptoms has been reported in several cardiovascular and non-cardiovascular diseases, such as myocardial infarction [9], heart failure [10], diabetes and hypertension [17,18]. On the contrary, several heart related disease may cause heart-rate turbulence which increase HRV [19]. As a result, a proper complexity in heart beat fluctuations has been accepted as a hallmark of healthy in physiology and is believed to reflect system adaptability in response to constant changes in internal and external inputs [20]. However, such statement needs more evidences and theory to explain the underlying phenomenon, otherwise, identifying the healthy and diseased state through the physiological fluctuations is more like a "blind men and elephant" approach.

1.3 Dynamical System and Orbits

From an engineer's perspective, the concept of the homeostasis can be represented by a complex feedback system and mathematically modeled as a dynamical system [21]. It can model the nonlinear feedback loops but not limited to feedback loops, actually, it has been widely used in many fields including biology and physiology. Often, the dynamic system model is in the form of a set of differential equations depicting the mechanistic interactions between components of the system are constructed:

$$\dot{\vec{u}} = \vec{f}(\vec{u}, \vec{P})$$

Here \vec{u} is an N dimensional vector describing the state of the system at any given time. \vec{f} is a vector field describing the dynamics of the system. Parameter vector \vec{P} and the vector field function \vec{f} together determine evolution rule of the dynamical system that describes what future states follow from the current state. The output of the model is the orbit (state function or trajectory), the path that state follows through space as a function of time. The orbits under the same model (the same vector field \vec{f}) will be different if started from different position. Among these possible orbits (realizations), different initial condition may leads to different outcome, therefore, the features on the vector field \vec{f} are more interest. Often, in a given system all orbits may tend to a point or a closed curve which constitutes an attractor for the system. By examining the state space in the neighborhood of a given attractor we can determine the basin of attraction for that attractor. For example, to simulation a ventricular cell one can use numerical integration of the Hodgkin-Huxley-type ionic model using a forward Euler scheme, with V at time $t + \Delta t$ calculated as:

$$V(t + \Delta t) = V(t) - (\Delta t / C_m) \sum I_i(t),$$

where C_m is membrane capacitance and I_i represents the individual ionic currents [22]. Lower figures are the simulation results in time domain (Figure 1, left) and in the phase plane (Figure 1, right).

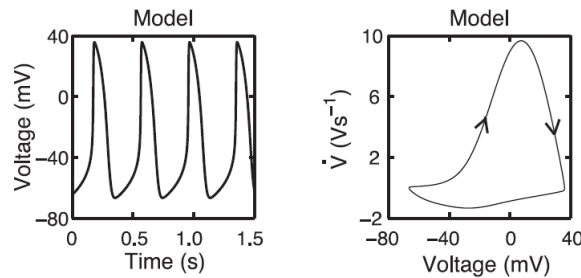
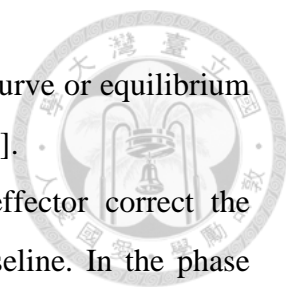


Figure 1 The voltage data and correspond phase-plane trajectory in the model

The orbits behave as a typical limit cycle nonlinear oscillator along with a closed curve attractor, the homeostasis on such model is dynamic equilibrium. If the parameters \vec{P} in the model is time independent, i.e. $\vec{P}(t) = \vec{P}$, the system is referred to as non-autonomous, otherwise, the system is autonomous. The time vary parameters $\vec{P}(t)$ thus can be used to model the environmental stimulus. As the autonomous system



disturbed by external stimulus, the orbit may shift from the closed curve or equilibrium point, and it may go back to the initial state after a period of time [23].

Recall the "set-point" concept of the control theory, as the effector correct the deviation by depressing it, the state variable will return to the baseline. In the phase plane, it acts like the orbit disturbed by a stimulus and finally converges to the equilibrium point (attractor or set-point). As a result, the concepts in homeostasis thus are related to the probability distribution of the orbits in the dynamical system model. In short, if paths of orbits are similar to each others, there will exist a attractor around them, and the nonlinear correlation between them are high. In other words, the similar but different path of orbits in the phase space implies the existing of governing rules of homeostatic control that "attract" the orbits". It also explained why a proper complexity in physiological fluctuations are neither random nor too regular under normal healthy conditions [20].

1.4 Reconstruct the Dynamics

Most control mechanisms are involved with the ANS which carries signals from the central nervous system to all organs of the body, in addition, the ANS regulates the function of most tissues and organs in the body [15]. As a result, it needs huge number of state variables involved in the regulations to describe the system completely. Without enough variables, it's really hard to know the whole picture describes the interactions between each components. Therefore, this raise a problems of knowing the properties of a dynamic system with limit information.

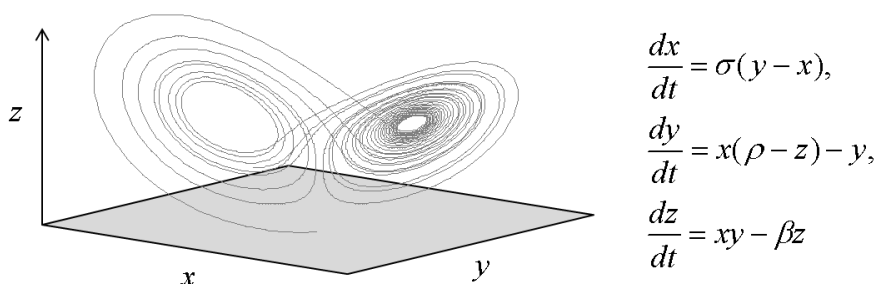


Figure 2 The Lorenz attractor and correspond differential equations

From Takens' Embedding theorem, "if we measure any single variable with

sufficient accuracy for a long period of time, it is possible to reconstruct the underlying dynamic structure of the entire system from the behavior of that single variable using delay coordinates and the embedding procedure” [25]. Figure 2 shows a well-known Lorenz attractor with the trajectory as a function of time $[x(t), y(t), z(t)]$ derived from the differential equations. By applying the embedding method on the $x(t)$, the time delayed series $[x(t), x(t-\tau), x(t-2\tau)]$ are plotted as figure 3 and the topological structure of the Lorenz attractor is preserved by the reconstruction.

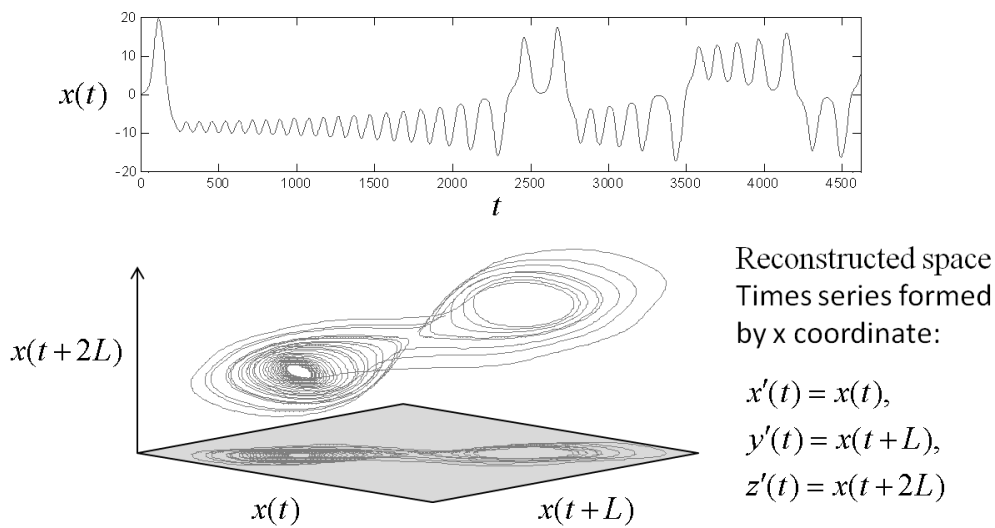


Figure 3 The time domain signal and the trajectory in reconstructed phase space

In 1983, Procaccia and Hentschel [26] described a numerical procedure to introduce a characteristic known now as the correlation dimension. As mention above, if paths of orbits are similar to each others, the nonlinear correlation between them are high. After that, sample-entropy and approximate-entropy have been proposed [27]. Because the correlations in the phase space can distinguish colored noise from deterministic chaotic behavior while the autocorrelation functions cannot [24], and the algorithm for correlation calculation is relatively simple and fast, such method has become one of the most popular characteristics of time series analysis.

However, the time scale of the physiological applications can range from several milliseconds to several days as mentioned earlier. The time lag L during the embedding procedure need to be defined first which is a trade-off between the small delay ($L = 1$) and the large delay ($L = 100$), as figure.4 shows. The Embedding theorem or correlation

dimension on certain time delay L fail to account for the multiple time scales inherent in time series (such as homeostatic system).

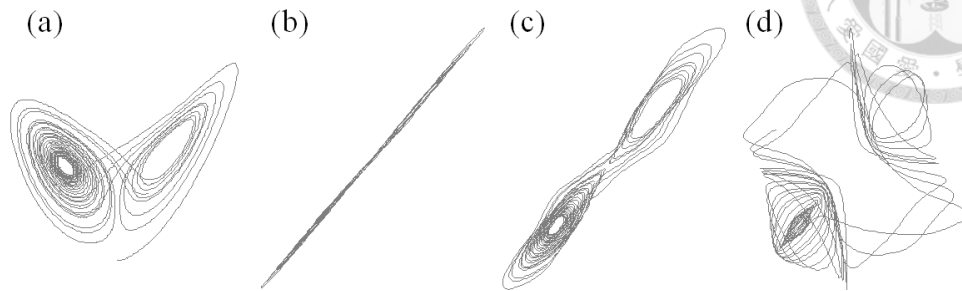
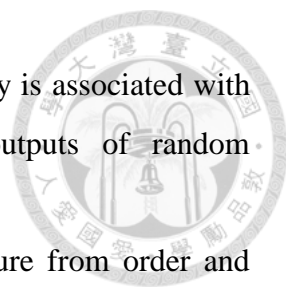


Figure 4 (a) the original phase plot and reconstructed phase space with different embedding delay L : (b) $L = 1$, (c) $L = 10$ and (d) $L = 100$ respectively. The delay parameter L determines the dimension of the reconstructed space and also the scales of fluctuations that can be seen on the reconstructed space.

1.5 Multiple Time Scale Dynamics

To solve this, the famous approach is the Multiscale Entropy Analysis (MSE) proposed by C.K. Peng in 2002 [11]. Through this method, complexity of a system could be derived from nonlinear correlations of variables at multiple time scales. The term "Entropy" has been defined as inversely related to energy (in the form of heat: $entropy = k \log D$) in the "Second Law" of classical thermodynamics, and commonly understood as a measure of disorder. Latter, Shannon and Weaver proposed the famous H measure: $H = -\sum p_i \ln p_i$, commonly understood as a measurement of uncertainty. However, neither the second law nor Shannon Entropy make distinction between living and non-living things.

In the book "What is Life?", Erwin Schrödinger proposed a controversial concept that life decreases or maintains its entropy by feeding on negative entropy [28]. The concept solve the conflict that life's dynamics may be argued to go against the tendency of second law due to the closed system. In other words, life tend to be highly ordered rather than unpredictable or random, the interactions between them should be correlated and meaningful which implies the entropy of life is low. But to maintain such order, life needs multiple scale structures and complex feedback paths [29]. Life thus become order and complex which may sound like an oxymoron, but this is due to mistaking the



meaning of complexity and randomness [21]. Intuitively, complexity is associated with “meaningful structural richness”, which, in contrast to the outputs of random phenomena, exhibits relatively higher regularity [20].

It thus raises a practical problem to distinguish complex structure from order and disordered systems. For this, MSE utilizes the entropy as a measuring tool for quantify the correlations in different time scales rather to directly use the entropy to "measure" the complexity. This turns the calculation into structural quantification which qualify the complexity in the way that more correlations in different time scale corresponds to more complex structures and more control mechanisms. As a result, the MSE method shows that correlated random signals (colored noise) are more complex than uncorrelated random signals (white noise) since the former has the correlations while the latter has not. The MSE use the averaging method to form new data series in coarse-graining steps (as figure 5 shows) and finally calculates the sample-entropy of each new series [20].

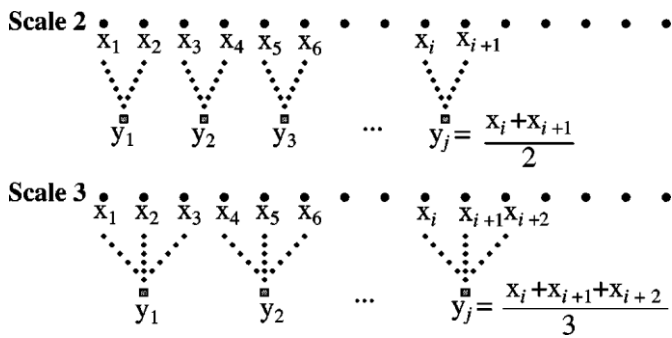
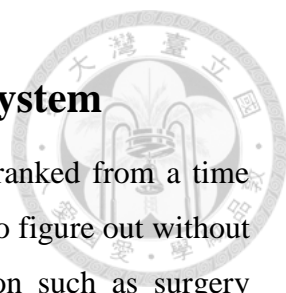


Figure 5 Coarse-graining steps for multiple scale entropy calculation

For MSE calculations, if time-lagged correlation exists in multiple time scales, it reflects that the system has complexity in structures with more adaptability in response to constant changes in internal and external inputs. Such concepts has been accepted as a hallmark of healthy physiological control and have been applied in many applications. However, most signal analysis in clinical applications are difficult to deal with, which always need modified methods to solve them, Chapter 2 will give two examples.



1.6 Attracting Orbit and Discrete Dynamical System

Although the complexity of a system can be reconstructed and ranked from a time series through MSE method, the underlying dynamics are still hard to figure out without the topological information. Furthermore, some clinical application such as surgery guiding needs spatial-temporal information for assessments, which is out of the scope of statistics analysis such as entropy based calculations.

Back to the nonlinear oscillator and attracting orbits in phase space mentioned above. There are several known periodic biological fluctuations that also fulfill the assumptions of attracting orbits in phase space, such as heart cycle, respiration cycle and circadian rhythm [30-32]. There are strict definitions of attracting orbits or periodic orbit in mathematics, but here we take the idea of the Poincaré map of a periodic orbit [33].

The stability of a periodic orbit in a dynamic system are usually calculated by the Poincaré map which replaces the n-dimensional continuous vector field with an (n-1) dimensional map, as figure 6 shows. Such map can be interpreted as a discrete dynamical system with a state space that is one dimension smaller than the original continuous dynamical system. Because it preserves many topological properties of periodic orbits of the original system and has a lower-dimensional state space it is often used for analyzing the original system [34].

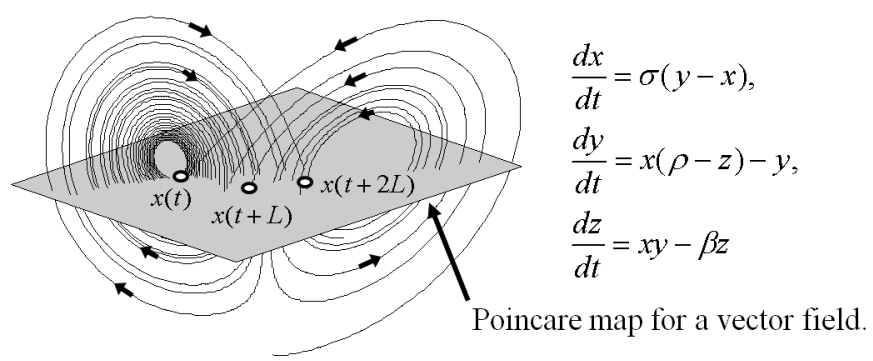


Figure 6 The discrete dynamical system derived from the intersection of the periodic orbits in a dynamic system.

Take the heart cycle as an example: the discrete dynamical system was firstly start on the R-wave peaks derived from the ECG signal. The cycle length dynamics then can be reconstructed through the n and (n+1) intervals in the Poincaré plot, as figure 7(b)

shows.

Second, the amplitude dynamics can be reconstructed directly through the time delayed embedded as shows in figure 7(c). The R-peaks in the reconstructed phase space thus become the discrete dynamical system that represented the amplitude variations of R-wave due to the respiratory effect (EDR), as shows in figure 7(d). Since the cycle length of the heart beats can be modulated by the respiratory, there are similarities in the distribution of these two different approaches (as figure 7(b) and (d) shows). The distribution on the Poincaré plot can be characterized by fitting an ellipse to it [35]. The length of axis 1 is defined as the SD of the plot data in that direction which describes the instantaneous beat-to-beat variability of the data, SD1. The length of axis 2 is defined as the SD of the plot data in the perpendicular direction, SD2, as figure 7(b) shows.

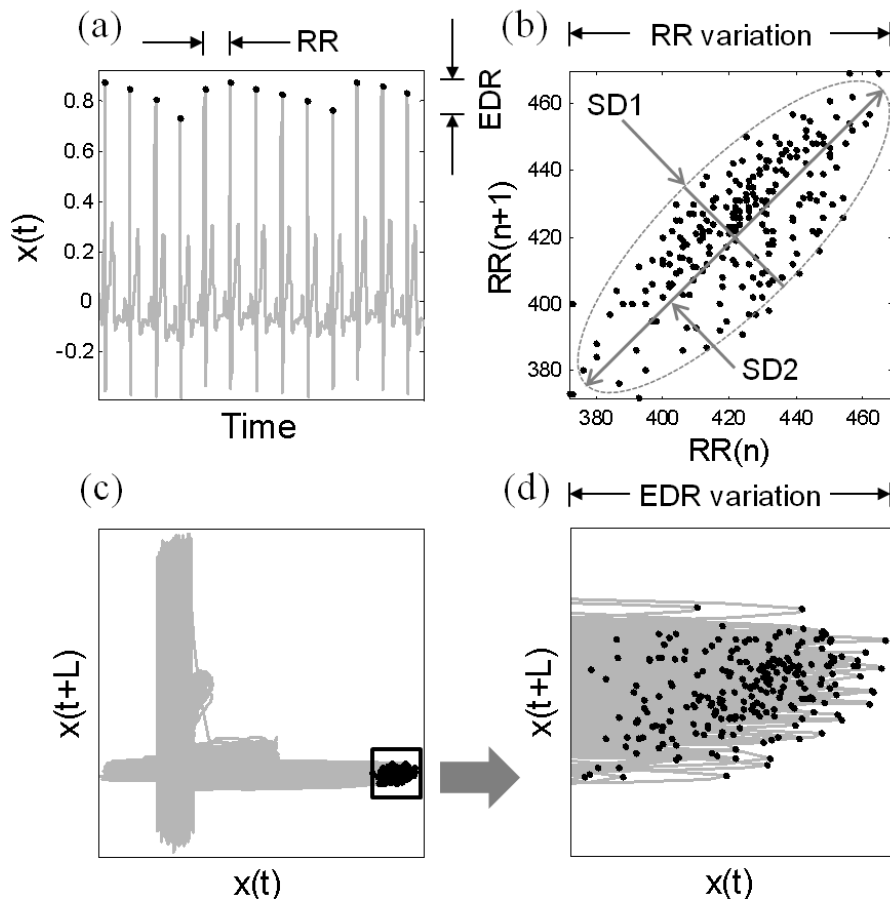



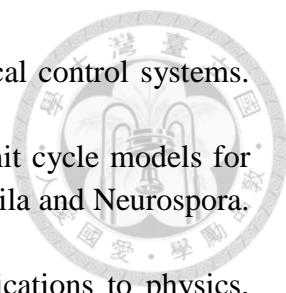
Figure 7 (a) ECG wave and correspond R-peak markers. (b) Poincaré plot of RR intervals. (c) The ECG signal and correspond R-peak markers on the reconstructed $\{x(t), x(t+L)\}$ space, the area of the markers is partially enlarged in (d).

This shows the attracting orbits can be reconstructed through different approaches, and each of them corresponds to different physiological meanings (cycle length or the amplitude of the peaks in ECG wave). Hence, the way to identify the feature points and the approach for reconstructed the discrete dynamical system would be the key. Chapter 3 will give two examples to explain how to identify the feature points from noisy data and quantify the attracting orbit from these points while the spatial-temporal information are still preserved.

REFERENCES

1. Cannon, W. B. Physiological Regulation of Normal States: Some Tentative Postulates Concerning Biological Homeostatics, Jubilee Volume for Charles Richet, Paris, 1926, p.91.
2. Cannon, W.B.. The Wisdom of the Body. New York: W. W. Norton & Company. 1932, pp. 177–201.
3. Marieb, Elaine Nicpon, and Katja Hoehn. Human anatomy & physiology. Pearson Education, 2007.
4. Davis, Graeme W. Homeostatic control of neural activity: from phenomenology to molecular design. *Annu. Rev. Neurosci.*, 2006, 29: 307-323.
5. Butcher, Eugene C.; Picker, Louis J. Lymphocyte homing and homeostasis. *Science*, 1996, 272.5258: 60-67.
6. Jilek and Prikrylova M. Jilek, D. Prikrylova. ,in: G.W. Hoffman, T. Immunology and Epidemiology, 65Springer-Verlag, 1985, pp. 8–14.
7. T. Wada, M. Jinnouchi, Y. Matsumura. Application of autoregressive modeling for the analysis of clinical and other biological data *Ann. Inst. Statist. Math.*, 40 1988, pp. 211–227
8. Buchman TG. Physiological stability and physiological state. *J Trauma*. 1996;41:599–605.
9. Kleiger RE, Miller JP, Bigger JT Jr, Moss AJ. (1987). "Decreased heart rate variability and its association with increased mortality after acute myocardial infarction". *Am J Cardiol*. 59 (4): 256–262.
10. Makikallio TH, Huikuri HV, Hintze U, Videbaek J, Mitrani RD, Castellanos A, Myerburg RJ, Moller M, Group DS: Fractal analysis and time- and frequency-domain measures of heart rate variability as predictors of mortality in patients with heart failure. *Am J Cardiol* 2001, 87:178–182.
11. Costa M, Goldberger AL, Peng CK: Multiscale entropy analysis of complex physiologic time series. *Phys Rev Lett* 2002, 89:068102.
12. Saykrs, B. McA. Analysis of heart rate variability. *Ergonomics*, 1973, 16.1: 17-32.
13. Cardiac Arrhythmias-Mechanisms, Pathophysiology, and Treatment. InTech, 2014.

- 
14. Malliani A, Pagani M, Lombardi F, Cerutti S. Cardiovascular neural regulation explored in the frequency domain. *Circulation*. 1991;84:482-492.
 15. Jänig, Wilfrid. *The integrative action of the autonomic nervous system: Neurobiology of homeostasis*. Cambridge University Press, 2006.
 16. Billman, George E. The LF/HF ratio does not accurately measure cardiac sympatho-vagal balance. *Frontiers in physiology*, 2013, 4.
 17. Gerritsen, J et al. Impaired autonomic function is associated with increased mortality, especially in subjects with diabetes, hypertension or a history of cardiovascular disease. *Diabetes Care* 2001;24
 18. Masi, C et al. Respiratory Sinus Arrhythmia and Diseases of Aging: Obesity, Diabetes Mellitus and Hypertension. *Biol Psychol* 2007;74(2):212-223.
 19. Bauer, Axel, et al. Heart rate turbulence: standards of measurement, physiological interpretation, and clinical use: International Society for Holter and Noninvasive Electrophysiology Consensus. *Journal of the American College of Cardiology*, 2008, 52.17: 1353-1365.
 20. Costa M, Goldberger AL, Peng CK: Multiscale entropy analysis of biological signals. *Phys Rev E Stat Nonlin Soft Matter Phys* 2005, 71:021906.
 21. Yates, F. Eugene. *Order and complexity in dynamical systems: homeodynamics as a generalized mechanics for biology*. Mathematical and computer modeling, 1994, 19.6: 49-74.
 22. Krogh-Madsen, Trine, et al. An ionic model for rhythmic activity in small clusters of embryonic chick ventricular cells. *American Journal of Physiology-Heart and Circulatory Physiology*, 2005, 289.1: H398-H413.
 23. Gabriella, Hegyi; Gyula, Vincze; Andras, Szasz. On the dynamic equilibrium in homeostasis. *Open Journal of Biophysics*, 2012, 2012.
 24. Sugihara, George; MAY, Robert M. Nonlinear forecasting as a way of distinguishing chaos from measurement error in time series. *Nature*, 1990, 344.6268: 734-741.
 25. F. Takens, in *Dynamical Systems and Turbulence*, edited by D. A. Rand and L. S. Young. *Lecture Notes in Mathematics Vol. 898* sSpringer, Berlin, 1981, p. 366.
 26. Hentschel, H. G. E.; Procaccia, Itamar. The infinite number of generalized dimensions of fractals and strange attractors. *Physica D: Nonlinear Phenomena*, 1983, 8.3: 435-444.
 27. Richman, Joshua S.; Moorman, J. Randall. Physiological time-series analysis using approximate entropy and sample entropy. *American Journal of Physiology-Heart and Circulatory Physiology*, 2000, 278.6: H2039-H2049.
 28. Schrodinger, Erwin; LEWIN. *What is life*. University Press, 1967.
 29. Buchman, Timothy G. The community of the self. *Nature*, 2002, 420.6912: 246-251.
 30. Mcsharry, Patrick E., et al. A dynamical model for generating synthetic electrocardiogram signals. *Biomedical Engineering, IEEE Transactions on*, 2003, 50.3: 289-294.

- 
31. Mackey, Michael C., et al. Oscillation and chaos in physiological control systems. *Science*, 1977, 197.4300: 287-289.
 32. Leloup, Jean-Christophe; Gonze, Didier; Goldbeter, Albert. Limit cycle models for circadian rhythms based on transcriptional regulation in *Drosophila* and *Neurospora*. *Journal of Biological Rhythms*, 1999, 14.6: 433-448.
 33. Strogatz, Steven H. *Nonlinear dynamics and chaos: with applications to physics, biology, chemistry, and engineering*. Westview press, 2014.
 34. Hirsch, Morris W.; Smale, Stephen; Devaney, Robert L. *Differential equations, dynamical systems, and an introduction to chaos*. Academic press, 2004.
 35. Huikuri, Heikki V., et al. Abnormalities in beat-to-beat dynamics of heart rate before the spontaneous onset of life-threatening ventricular tachyarrhythmias in patients with prior myocardial infarction. *Circulation*, 1996, 93.10: 1836-1844.



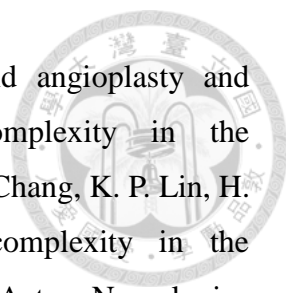
Chapter 2

Quantization of Multi-scale correlation

2.1 Application of a Refined Entropy Computational Method in Assessing Complexity of Pulse Wave Velocity Signals in Healthy and Diabetic Subjects

2.1.1 INTRODUCTION

Atherosclerosis, which is the major pathological change underlying most cardiovascular diseases, has been reported to be associated with advanced age, history of stroke, diabetes, hypertension, and cerebrovascular disease. Pulse wave velocity (PWV) is one of the most popular non-invasive parameter for the assessment of atherosclerosis. Despite different equipment used for data acquisition, a mean value is usually obtained from the examinee for evaluating the severity of the condition (Blacher, Asmar et al. 1999; Laurent, Boutouyrie et al. 2001; Yamashina, Tomiyama et al. 2002; Mitchell, Parise et al. 2004; Tsai, Chen et al. 2005; Wu, Hsu et al. 2012). On the other hand, Costa et al. found healthy subjects and those with heart conditions can be reliably differentiated by a simple measure based on the thermodynamical concept of “entropy” (Costa, Goldberger et al. 2002). “Multi-scale entropy (MSE)” is a non-linear means of assessing the complexity of physiological signals (Costa, Goldberger et al. 2002; Costa and Healey 2003; Costa, Peng et al. 2003). Compared to the traditional complexity measures, MSE has the advantage of being applicable to both physiologic and physiologic signals of finite length. MSE, which was first reported by Costa et al. to compare the differences in R-R interval (RRI) among healthy subjects, patients with atrial fibrillation and those with congestive heart failure (CHF) (Costa, Goldberger et al. 2002), has been successfully applied to the interpretation of physiological series and data from patients with various diseases. In previous studies, MSE provided the best prognostic prediction in patients with congestive heart failure (CHF) (Ho YL, Lin C, Lin YH, Lo MT. The prognostic value of non-linear analysis of heart rate variability in patients with congestive heart failure--a pilot study of multiscale entropy. PloS one



2011;6:e18699.) and patients receiving unilateral primary carotid angioplasty and stenting were reported to exhibit acute increase of complexity in the neurocardiovascular dynamics (H. K. Yuan, C. Lin, P. H. Tsai, F. C. Chang, K. P. Lin, H. H. Hu, M. C. Su, and M. T. Lo, "Acute increase of complexity in the neurocardiovascular dynamics following carotid stenting," *Acta Neurologica Scandinavica*, vol. 123, pp. 187-192, 2011.). In 2006, Escudero et al. reported significant difference in entropy values from signals of electroencephalograms (EEG) between healthy individuals and those with Alzheimer's disease after data processing with MSE (Escudero, Abásolo et al. 2006). Accordingly, we have previously shown that healthy, aged, and diabetic subjects can be distinguished with MSE using 1000 successive PWV signals with a scale factor of 10 (Wu, Hsu et al. 2011). Despite being reliable, the whole recording process takes up to 30 minutes that is usually not well tolerated by aged or diseased subjects (Wu, Hsu et al. 2011).

To refine the assessment approach, the present study proposes a novel means of computation, "short time multiscale entropy (sMSE)", in an attempt to reduce the time for data acquisition through refined computation of the harvested data. To compare between MSE and sMSE in terms of their sensitivity and validity in differentiating signals of small sample size and among healthy, aged, and diabetic subjects, both simulation signals and PWV data from testing subjects were used for the current study.

2.1.2 METHODS

Subject Population and Grouping

The testing subjects were divided into four groups, including healthy young individuals of age between 20 and 40 (Group 1, n =24), healthy aged subjects of age between 20 to 40 (Group 2, n =30), middle-aged patients with well-controlled diabetes mellitus type 2 [Defined as age between 41 to 80 and $6.5\% < \text{glycosylated hemoglobin (HbA1c) level} < 8.0\%$] (Group 3, n =18), and middle-aged patients with poorly-controlled diabetes mellitus type 2 (Defined as age between 41 to 80 with $\text{HbA1c level} \geq 8.0\%$) (Group 4, n = 22). All participants were volunteers. Diabetic patients, who were recruited from the diabetic outpatient clinic of Hualien Hospital from July 2009 to October 2010, fit all the three criteria of (1) Fasting blood sugar $>126\text{mg/dL}$, (2) $\text{HbA1c level} > 6.5\%$, and (3) Established diagnosis of diabetes mellitus

type 2 with a follow-up period > 2 years. On the other hand, healthy subjects, who were recruited from the health screening clinic of Hualien hospital during the same period, had to fill out a questionnaire declaring the absence of medical history of cardiovascular diseases (i.e. Stroke, hypertension, diabetes). The whole study has been approved by the Institutional Review Board (IRB) of Hualien Hospital and National Dong Hwa University. Informed consents were signed by all testing subjects.

Short Time Multiscale Entropy (sMSE)

The original MSE comprises of two steps: 1) coarse-graining the signals using different time scales; 2) quantifying the degree of irregularity in each coarse-grained time series using sample entropy (SampEn). However, the major challenge of of MSE in clinical application is the need of massive data for the reliability.

Short time multiscale entropy (sMSE) is a novel approach of computation that enables the use of large scale factor for analysis on data acquired through a shortened time period. The basic concept is the creation of different time series through removing a small number of recordings from the beginning without affecting the overall trend and complexity of the acquired signals. The acquired time series then undergo Sample Entropy (SE)(Richman and Moorman 2000) computation with steady values of entropy obtained (Figure.1).

Through altering the number of Lag from 0 to L (where $L = \tau - 1$, $\tau =$ coarse-grained scale factor) on the native time series (1), a new time series, $T^{(p)}$, can be obtained (2). Thus, the number of new time series generated is $L+1$.

$$T_N = \{X_1, X_2, \dots, X_{N-1}, X_N\} \quad (1)$$

$$T^{(p)} = \{X_k, X_{k+1}, X_{k+2}, \dots, X_{N-1}, X_N\}, k=p+1, p=0,1,2,\dots,L \quad (2)$$

The $L+1$ time series acquired then undergo coarse-grained processing with a scale factor τ (3), giving the time series of $y^{(p)(\tau)}$. Hence

$$y_j^{(p)(\tau)} = \frac{1}{\tau} \sum_{k=(j-1)\tau+1}^{j\tau+p} X_k, 1 \leq j \leq \left\lfloor \frac{N-p}{\tau} \right\rfloor, p=0,1,2,\dots,L \quad (3)$$

The $L+1 y^{(p)(\tau)}$ are then subjected to Sample Entropy computation and averaged, giving $sMSE_\tau$ of scale factor τ (4)

$$sMSE_\tau = \frac{1}{L+1} \sum_{p=0}^L SE(y^{(p)}(\tau)) \quad (4)$$

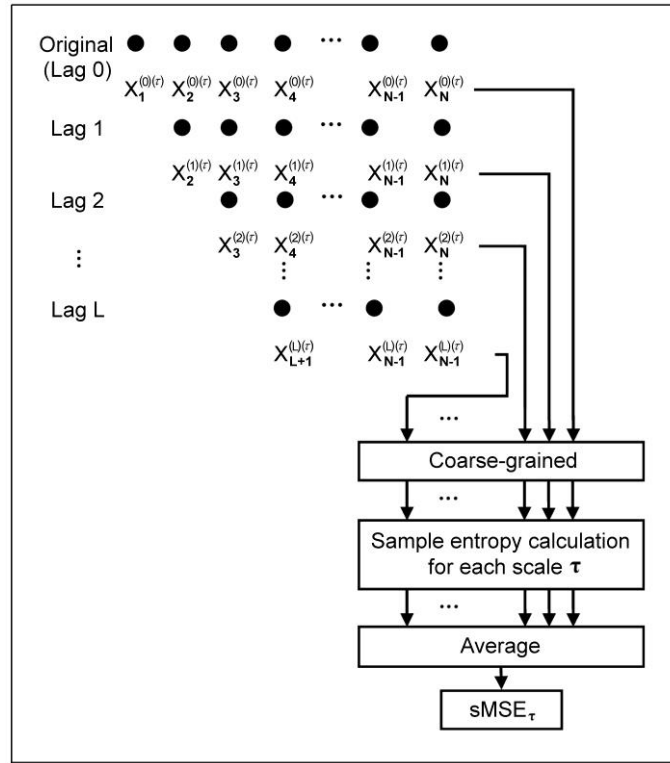


Figure 1. Method of short time multi-scale entropy (sMSE) computation

Short Time Multi-scale Entropy Index (sMEI) Using PWV Series

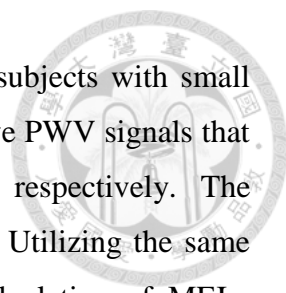
The results of MSE from 1000 successive PWV signals were compared with those of sMSE acquired from computation on the first 600 PWV signals using the novel computation approach in the current study. Utilizing a scale factor of 10, the present study categorized scale factors into short time multi-scale entropy index with small scale (sMEI_{SS}, scale1 to scale5) (5) and short time multi-scale entropy index with large scale (sMEI_{LS}, scale 6 to scale 10) (6) that were used to compare with the respective values of MEI_{SS} and MEI_{LS} from our previous study using MSE (Wu, Hsu et al. 2011).

$$sMEI_{SS} = 10 \left(\sum_{\tau=1}^5 sMSE_{\tau} \right) \quad (5)$$

$$sMEI_{LS} = 10 \left(\sum_{\tau=6}^{10} sMSE_{\tau} \right) \quad (6)$$

Study Design

The study comprised two parts. The first part involved the design of the sMSE method with simulation signals of white noise and 1/f noise using the MATLAB R2008b package (MathWorks, Natick, Massachusetts, U.S.A.). The second part focused



on computation of PWV-based multiscale entropy index in study subjects with small scale and that with large scale using MSE method on 1000 successive PWV signals that are referred to as $MEI_{SS} (PWV_{1000})$ and $MEI_{LS} (PWV_{1000})$, respectively. The computation has been previously described (Wu, Hsu et al. 2011). Utilizing the same approach, 600 successive PWV signals were obtained for the calculation of $MEI_{SS} (PWV_{600})$ and $MEI_{LS} (PWV_{600})$. Comparisons were first made between $MEI_{SS} (PWV_{1000})$ and $MEI_{SS} (PWV_{600})$ as well as between $MEI_{LS} (PWV_{1000})$ and $MEI_{LS} (PWV_{600})$ to study if a reduction in available data would affect the ability of differentiation among different groups. In addition, $MEI_{SS} (PWV_{600})$ and $MEI_{LS} (PWV_{600})$ were compared with $sMEI_{SS} (PWV_{600})$ and $sMEI_{LS} (PWV_{600})$, respectively, to investigate possible enhancement in sensitivities using the novel method for data processing.

Statistical Analysis

Average values are expressed as mean \pm SD. Statistical Package for the Social Science (SPSS, version 14.0 for Windows, SPSS Inc., Chicago, IL) was used for statistical analysis. Independent t-test was adopted for the determination of the significance of difference in study parameters among different groups. A probability value, p , of <0.05 represents statistical significance.

2.1.3 RESULTS

Computation of Sample Entropy Using Multi-Scale Entropy (MSE) and Short Time Multi-Scale Entropy (sMSE) methods on Simulation Signals

Values of sample entropy were acquired through multi-scale entropy (MSE) (Figure 2a) and short time multi-scale entropy (sMSE) (Figure 2b) methods using simulation white noise and 1/f noise with different scale factors on 30 sets of 1000 successive signals. The results showed that the values of sample entropy decreased with an increase in values of the coarse grained scale factor regardless of the method used. On the other hand, computation with 1/f noise eliminated the effect of scale factor, giving a value of around 2 for both methods (Figure 2a & 2b). Comparison of changes in values of sample entropy using multi-scale entropy (MSE) and short time multi-scale entropy (sMSE) approaches with different scale factors on 600 successive white noise signals (Figure 3) showed a steady drop in sample entropy as the scale factor increased from 1 to 4. From the scale factor 5 onwards, sample entropy from MSE began to exhibit

remarkable fluctuations, while that from sMSE showed a relatively steady decrease.

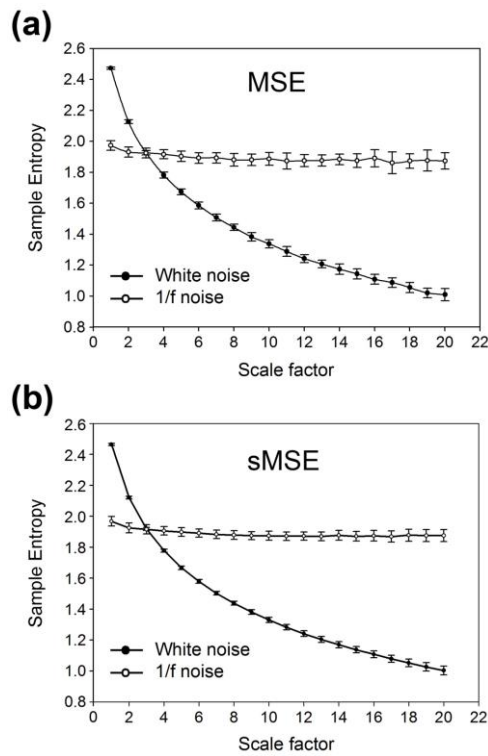


Figure 2. Simulation signals. (a) Values of sample entropy acquired through multi-scale entropy (MSE) computation using white noise and 1/noise with different scale factors on 30 sets of 1000 successive signals. (b) Values of sample entropy acquired through short-time multi-scale entropy (sMSE) computation using white noise and 1/noise with different scale factors on 30 sets of 1000 successive signals

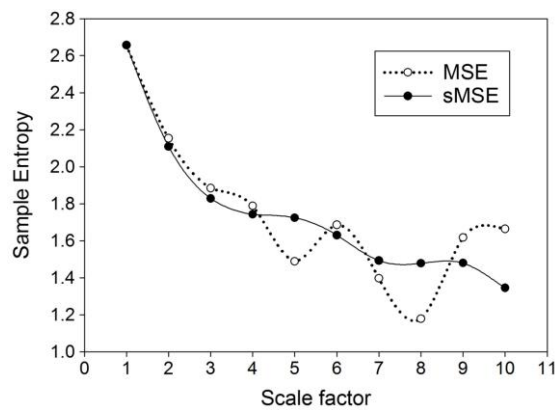


Figure 3. Comparison of changes in values of sample entropy using multi-scale entropy (MSE) and short time multi-scale entropy (sMSE) methods with different scale factors on 600 successive white noise signals

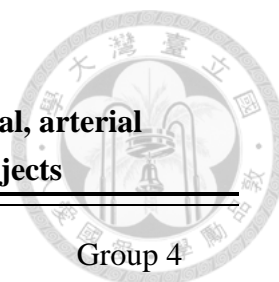


Table 1
Comparison of anthropometric, hemodynamic, serum biochemical, arterial stiffness, and multiple entropy parameters among the testing subjects

Parameter	Group 1	Group 2	Group 3	Group 4
600 points				
Number	24	30	18	22
Ages (years)	25.8±5.6	52.6±6.6**	56.5±9.3	57.9±9.5
Duration of Diabetes(years)	0	0	6.8±3.8	11.7±6.8 ⁺⁺
circumference(cm)	79.9±10.8	84.3±10.1	92.2±10.1 ^e	96.7±12.8
BMI (kg/m ²)	22.6±3.5	24.2±3.9	26.9±3.7	28.4±5.2
SBP (mmHg)	115.5±9.8	115.5±14.4	129.8±22.0 ^e	125.7±19.4
DBP(mmHg)	70.1±6.6	73.9±10.0	78.5±13.6	75.5±10.8
PP(mmHg)	44.5±6.6	41.1±9.4	51.2±12.3 ^e	45.1±6.7
HbA1c(%)	5.5±0.2	5.8±0.4 [*]	6.8±0.7 ^{ee}	9.53±1.9 ⁺⁺
HDL(mg/dL)	41.7±11.5	49.4±14.1	39.9±11.4	43.2±14.9
Triglyceride (mg/dL)	100.6±74.0	106.0±54.9	107.0±51.7	156.9±74.3 ⁺
Fasting Blood Sugar(mg/dL)	92.4±8.4	96.1±9.9	128.5±28.1 ^{ee}	182.8±61.9 ⁺
PWV ₁₀₀₀ (m/s)	4.4±0.3	4.7±0.4 [*]	5.0±0.3 ^e	5.1±0.6
MEI _{SS} (PWV ₁₀₀₀)	96.5±4.4	97.4±4.3	98.4±6.7	91.5±12.5 ⁺
MEI _{LS} (PWV ₁₀₀₀)	89.4±7.3	84.3±6.3 [*]	79.6±9.2 ^e	71.9±12.6 ⁺
MEI _{SS} (PWV ₆₀₀)	97.0±7.6	99.1±4.3	100.9±8.3	93.3±12.4 ⁺
MEI _{LS} (PWV ₆₀₀)	88.3±10.8	86.1±12.8	85.2±11.0	82.9±11.6
sMEI _{SS} (PWV ₆₀₀)	95.9±10.0	96.8±7.1	96.9±11.3	89.2±12.1 ⁺
sMEI _{LS} (PWV ₆₀₀)	92.2±8.9	86.8±11.3 [*]	80.5±6.2 ^e	73.7±11.4 ⁺

Group 1: Healthy young subjects without known cardiovascular disease; Group 2: Healthy middle-aged subjects without known cardiovascular disease; Group 3: Middle-aged individuals with well-controlled diabetes mellitus type 2; Group 4: Middle-aged patients with poorly-controlled diabetes mellitus type 2. Values are expressed as mean±SD. BMI=body mass index; SBP=systolic blood pressure; DBP=diastolic blood pressure; PP=pulse pressure; HbA1c=glycosylated hemoglobin; HDL=high-density lipoprotein; PWV₁₀₀₀=1000 successive pulse wave velocity using the distance from the sternal to the second toe divided by the time difference between R wave on Lead II of ECG to the corresponding foot point of pulse wave of second toe; MEI_{SS} (PWV₁₀₀₀)= 1000 successive PWV-based multiscale entropy index with small scale; MEI_{LS} (PWV₁₀₀₀) = 1000 successive PWV-based multiscale entropy index with large scale; MEI_{SS} (PWV₆₀₀)= 600 successive PWV-based multiscale entropy index with small

scale; MEI_{LS} (PWV₆₀₀)= 600 successive PWV-based multiscale entropy index with large scale; sMEI_{SS} (PWV₆₀₀)= 600 successive PWV-based short time multiscale entropy index with small scale; sMEI_{LS} (PWV₆₀₀)= 600 successive PWV-based short time multiscale entropy index with large scale.

*p<0.05 Group 1 & Group 2, ^εp<0.05:Group 2 & Group 3, ⁺p<0.05:Group 3 & Group 4, **p<0.001 Group 1 & Group 2, ^{εε}p<0.001:Group 2 & Group 3, ⁺⁺p<0.001:Group 3 & Group 4

Demographic and Biochemical Parameters

Subjects in Group 3 was significantly older than those in Group 2 who, in turn, were significantly older than those in Group 1 (all p<0.001) (Table 1). The duration of diagnosed diabetes was significantly longer in Group 4 than that in Group 3 (p<0.001). Although there was no significant difference in body mass index (BMI) among the four groups, the waist circumference was significantly larger with systolic blood pressure higher in individuals in Group 3 compared to those in Group 2 (both p=0.005). Besides, the pulse pressure was also substantially higher in Group 3 than that in Group 2 (p=0.001). Moreover, the levels of HbA1c were significantly different among the four groups with Group 4 being the highest, followed by Group 3, Group 2, and Group 1 (Group 1 vs. Group 2, p=0.007; Group 2 vs. Group 3 & Group 3 vs. Group 4, p<0.001), although the parameter was within normal range (i.e. <6.0%) in Group 1 and Group 2. Serum triglyceride was also significantly higher in Group 4 than in Group 3 (p=0.037). Furthermore, fasting blood sugar level was highest in Group 4, followed by Group 3 and Group 2, while there was no notable difference between Group 1 and Group 2 (Group 2 vs. Group 3, p<0.001; Group 3 vs. Group 4, p=0.003).

Comparisons among PWV1000, MEISS (PWV1000), MEILS (PWV1000), MEISS (PWV600), MEILS (PWV600), sMEISS (PWV600) and sMEILS (PWV600)

PWV₁₀₀₀ was lowest in Group 1, followed by that of Group 2 and Group 3, while there was no remarkable difference in this parameter between Group 3 and Group 4 (Group 1 vs. Group 2, p=0.007; Group 2 vs. Group 3, p=0.009). MEI_{SS} (PWV₁₀₀₀) was significantly higher in Group 3 than that in Group 4 (p=0.02). On the other hand, MEI_{LS} (PWV₁₀₀₀) was higher in Group 1 than that in Group 2 (p=0.03), significantly higher in Group 2 than that in Group 3 (p=0.016), and higher in Group 3 compared to that in Group 4 (p=0.04). Although MEI_{SS} (PWV₆₀₀) was significantly higher in Group 3 than that in Group 4 (p=0.005), there was no significant difference in MEI_{SS} (PWV₆₀₀) between Group 1 and Group 2. Failure in differentiation was noted between Group 1

and Group 2 using MEI_{SS} (PWV₆₀₀) as well as among Groups 2, 3, and 4 using MEI_{LS} (PWV₆₀₀). Similar to that of MEI_{SS} (PWV₆₀₀), although sMEI_{SS} (PWV₆₀₀) was significantly higher in Group 3 than that in Group 4 ($p=0.011$), it failed to differentiate among Groups 1, 2, and 3. On the other hand, sMEI_{LS} (PWV₆₀₀) was significantly higher in Group 1 than that in Group 2 ($p=0.029$), higher in Group 2 than that in Group 3 ($p=0.045$), and higher in Group 3 than that in Group 4 ($p=0.045$).

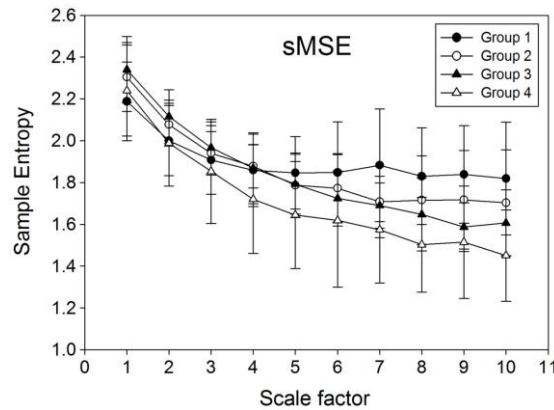
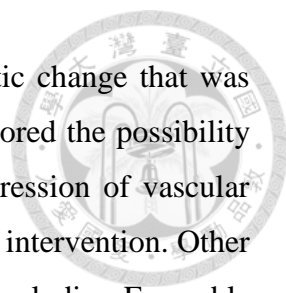


Figure 4. Values of sample entropy obtained through computation using short time multi-scale entropy (sMSE) method on 600 successive pulse wave velocity (PWV) signals. Group 1: Healthy young subjects without known cardiovascular disease; Group 2: Healthy middle-aged subjects without known cardiovascular disease; Group 3: Middle-aged individuals with well-controlled diabetes mellitus type 2; Group 4: Middle-aged patients with poorly-controlled diabetes mellitus type 2

There was an overall reduction in sample entropy with an increase in scale factors (Figure 4). While no significant difference among the four groups was noted on a scale factor less than 6, significant differences began to emerge when the scale factor was 6 or above. The value of sample entropy was highest in Group 1, followed by that of Group 2, Group 3, and Group 4.

2.1.4 DISCUSSION

PWV is one of the most popular noninvasive assessment tools for the assessment of atherosclerosis (Laurent, Boutouyrie et al. 2001; Tsai, Chen et al. 2005; Cecelja and Chowienczyk 2009) that operates on the assumption that PWV is a stationary parameter. However, after analyzing the data on PWV over 1000 cardiac cycles within 30 minutes, our previous study (Wu, Hsu et al. 2011) demonstrated that PWV is a non-stationary



parameter, the variability of which may reflect subtle atherosclerotic change that was missed by taking only the mean value for analysis. That study explored the possibility of combining MSE and PWV in assessing sugar control and progression of vascular pathology in diabetic patients and elderly to allow timely therapeutic intervention. Other than MSE, various tools for non-linear data analysis are available, including Ensemble empirical Mode Decomposition (EEMD) (Wu and Huang 2009; Chang and Liu 2011), linguistic (Yang, Hseu et al. 2003; Lei, Li et al. 2007) and fractal (Goldberger, Amaral et al. 2002; Tapanainen, Thomsen et al. 2002) analyses.

Albeit sensitive in differentiating healthy, aged, and diabetic subjects, one of the pitfalls of applying MSE for PWV signal analysis is the relatively long time for data collection that involves the acquisition of 1000 successive signals in 30 minutes (Wu, Hsu et al. 2011). Our experience showed that, although a scale factor of 10 can be used for analyzing 1000 successive PWV signals to produce significant outcomes, the use of scale factor 10 on a smaller sample size acquired within a shorter time period would give aberrant results (Figure 3). In an attempt to solve the problem, the current study introduced a novel non-linear computational method, sMSE, that gave values of sample entropy comparable to those obtained through MSE from a relatively long period of simulation signals (Figure 2a & 2b). The results, therefore, are consistent with those from the study of Peng et al. that also demonstrated similar results in simulation study on healthy subjects and those with cardiac diseases (Costa, Goldberger et al. 2005). Using a relatively small simulation sample size of 600, the changes in sample entropy acquired with MSE and sMSE were compared (Figure 3). The results showed spiking increases in entropy at a scale factor of 6, 9, and 10 using the MSE method, while sample entropy from sMSE exhibited a relatively steady reduction throughout the elevation in scale factor from 1 to 10. Compared to traditional MSE, the significantly reduced standard deviation of sMSE indicates the reduction of the cost of the experimentation. Therefore, despite a smaller sample size, sMSE could still produce results similar to that of MSE on a large sample (Figure 2a). The results highlight the applicability of sMSE in the analysis of signals acquired through a long time period and also those from a relatively short period (i.e. 600 consecutive signals) using a scale factor of 10 to produce steady results that could not be obtained through the original MSE approach. The results from simulation studies are consistent with those from human subjects. Although MEI_{SS} (PWV_{600}) and MEI_{LS} (PWV_{600}) failed to reproduce the

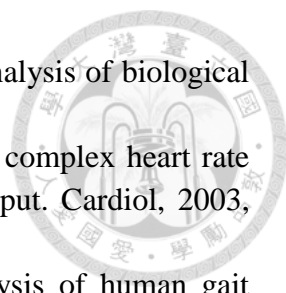
significant results from MEI_{SS} (PWV_{1000}) and MEI_{LS} (PWV_{1000}) after curtailing the sampling size, $sMEI_{SS}$ (PWV_{600}) and $sMEI_{LS}$ (PWV_{600}) were found to be as sensitive as MEI_{SS} (PWV_{1000}) and MEI_{LS} (PWV_{1000}) in differentiating among the four groups. Failure in differentiation among the four groups using MEI_{LS} (PWV_{600}) (Table 1) may be due to the marked fluctuations in sample entropy at large scale factors (Figure 3). Furthermore, consistent with the findings of previous studies (Wu, Hsu et al. 2011), the results of the present study also demonstrated a reduction in signal complexity with age and the severity of diabetes (Figure 4).

The present study has its limitations. First, compared with MSE, the method of sMSE requires a larger volume of computation. Second, although we have established a signal-to-scale factor ratio of 100 (i.e. 1000 successive signals/ scale factor 10) as a minimal requirement for successful computation using the MSE approach and a reduced ratio of 60 for sMSE in this study, whether aberrancy would arise from sMSE using a ratio below 60 remains to be elucidated.

In conclusion, the present study demonstrated that, using a novel sMSE approach for PWV signal analysis, the time for data acquisition can be substantially reduced from 30 minutes to 10 minutes with remarkable preservation of sensitivity in differentiating among the healthy, aged, and diabetic populations compared with the conventional MSE method.

REFERENCES

1. Blacher, J., R. Asmar, et al. (1999). Aortic pulse wave velocity as a marker of cardiovascular risk in hypertensive patients. *Hypertension.*, 33, 1111-1117.
2. Cecelja, M. and P. Chowienczyk (2009). Dissociation of aortic pulse wave velocity with risk factors for cardiovascular disease other than hypertension a systematic review. *Hypertension.*, 54, 1328-1336.
3. Chang, K.-M. and S.-H. Liu (2011). Gaussian noise filtering from ECG by Wiener filter and ensemble empirical mode decomposition. *J. Signal. Process. Syst.*, 64, 249-264.
4. Costa, M., A. Goldberger, et al. (2002). Multiscale entropy to distinguish physiologic and synthetic RR time series. *Comput. Cardiol*, 2002, IEEE.
5. Costa, M., A. L. Goldberger, et al. (2002). Multiscale entropy analysis of complex physiologic time series. *Phys. Rev. Lett.*, 89, 068102.

- 
6. Costa, M., A. L. Goldberger, et al. (2005). Multiscale entropy analysis of biological signals. *Phys. Rev.E* ., 71, 021906.
 7. Costa, M. and J. Healey (2003). Multiscale entropy analysis of complex heart rate dynamics: discrimination of age and heart failure effects. *Comput. Cardiol*, 2003, IEEE.
 8. Costa, M., C.-K. Peng, et al. (2003). Multiscale entropy analysis of human gait dynamics. *Physica A* ., 330, 53-60.
 9. Escudero, J., D. Abásolo, et al. (2006). Analysis of electroencephalograms in Alzheimer's disease patients with multiscale entropy. *Physiol. Meas*, 27, 1091.
 10. Goldberger, A. L., L. A. Amaral, et al. (2002). Fractal dynamics in physiology: alterations with disease and aging. *Proc. Natl. Acad. Sci. U. S. A.*, 99, 2466-2472.
 11. Laurent, S., P. Boutouyrie, et al. (2001). Aortic stiffness is an independent predictor of all-cause and cardiovascular mortality in hypertensive patients. *Hypertension*., 37, 1236-1241.
 12. Lei, W. K., B. N. Li, et al. (2007). AFC-ECG: an adaptive fuzzy ECG classifier. *Soft Computing in Industrial Applications*, Springer: 189-199.
 13. Mitchell, G. F., H. Parise, et al. (2004). Changes in arterial stiffness and wave reflection with advancing age in healthy men and women the Framingham Heart Study. *Hypertension*., 43, 1239-1245.
 14. Richman, J. S. and J. R. Moorman (2000). Physiological time-series analysis using approximate entropy and sample entropy. *Am. J. Physiol. Heart. Circ. Physiol.*, 278, H2039-H2049.
 15. Tapanainen, J. M., P. E. B. Thomsen, et al. (2002). Fractal analysis of heart rate variability and mortality after an acute myocardial infarction. *Am. J. Cardiol.*, 90, 347-352.
 16. Tsai, W.-C., J.-Y. Chen, et al. (2005). Association of Risk Factors With Increased Pulse Wave Velocity Detected by a Novel Method Using Dual-Channel Photoplethysmography*. *Am. J. Hypertens.*, 18, 1118-1122.
 17. Wu, H.-T., P.-C. Hsu, et al. (2011). Multiscale entropy analysis of pulse wave velocity for assessing atherosclerosis in the aged and diabetic. *Biomedical Engineering, IEEE Transactions*., 58, 2978-2981.
 18. Wu, H.-T., P.-C. Hsu, et al. (2012). Six-channel ECG-based pulse wave velocity for assessing whole-body arterial stiffness. *Blood Pressure*., 21, 167-176.
 19. Wu, Z. and N. E. Huang (2009). Ensemble empirical mode decomposition: a noise-assisted data analysis method. *Adv. Adapt. Data. Anal.*, 1, 1-41.
 20. Yamashina, A., H. Tomiyama, et al. (2002). Validity, reproducibility, and clinical significance of noninvasive brachial-ankle pulse wave velocity measurement. *Hypertens. Res.*, 25, 359-364.
 21. Yang, A. C.-C., S.-S. Hseu, et al. (2003). Linguistic analysis of the human heartbeat using frequency and rank order statistics. *Phys. Rev. Lett.*, 90, 108103.

2.2 Outlier-Resilient Complexity Analysis of Heartbeat Dynamics

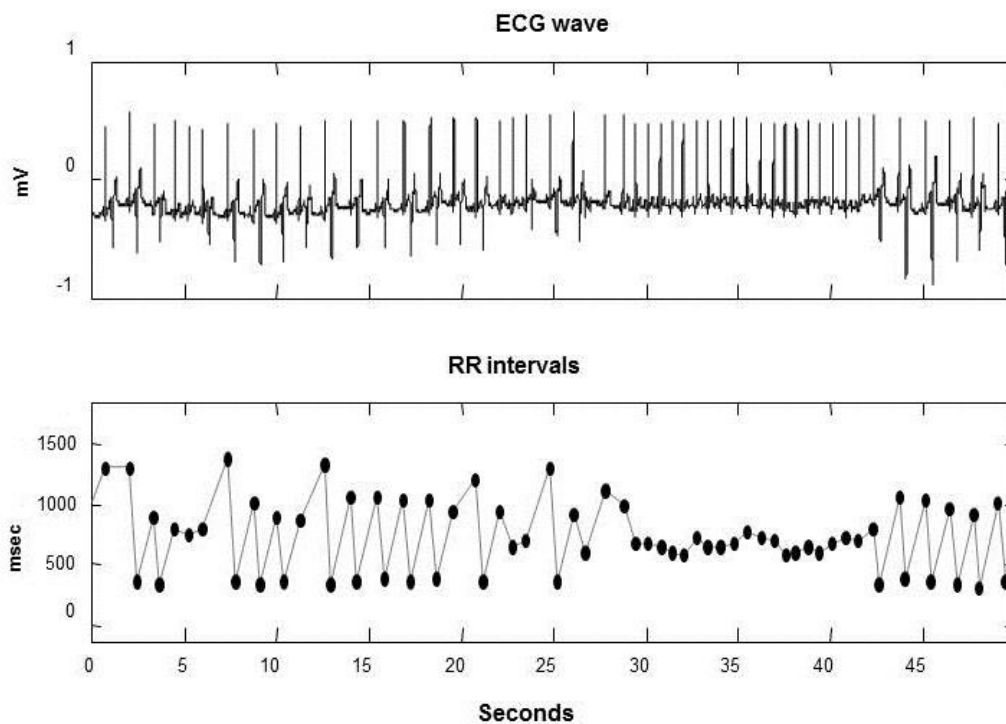


2.2.1 INTRODUCTION

Complexity in physiological outputs is believed to be a hallmark of healthy physiological control. How to accurately quantify the degree of complexity in physiological signals with outliers remains a major barrier for translating this novel concept of nonlinear dynamic theory to clinical practice. Here we propose a new approach to estimate the complexity in a signal by analyzing the irregularity of the signal time series of its coarse-grained time series at different time scales. Using surrogate data, we show that the method can reliably assess the complexity in noisy data while being highly resilient to outliers. We further apply this method on human heartbeat recordings. Without removing any outliers due to ectopic beats, the method is able to detect a degradation of cardiac control in patients with congestive heart failure and a more degradation in critically ill patients whose life continuation relies on extracorporeal membrane oxygenator (ECMO). Moreover, the derived complexity measures can predict the mortality of ECMO patients. These results indicate that the proposed method may serve as a promising tool for monitoring cardiac function of patients in clinical settings. Many physiological variables such as motor activity and heart rate display seemingly irregular fluctuations over a wide range of time scales^{1,2}. Under normal healthy conditions, these physiological fluctuations are neither random nor too regular, possessing robust, multi-scale dynamic patterns that are independent of external influences³⁻⁵. Such a complexity in physiological fluctuations has been accepted as a hallmark of healthy physiology and is believed to reflect system adaptability in response to constant changes in internal and external inputs. Numerous studies have supported this theory of complexity by showing that physiological fluctuations become either too random or too regular with aging and under pathological breakdowns⁶⁻¹⁰.

Despite the physiological importance of the complexity theory, its application to clinical studies has been hindered by the lack of algorithms that can be easily implemented for accurate estimation of the degree of complexity in physiological fluctuations^{3,4}. One generic challenge for algorithm design is to account for the effects of “outliers”, which often exist in clinical recordings due to not only external random

influences but also intrinsic physiological/pathological incidence such as ectopic beats in ECG recordings 5 (Figure 1). For example, multiscale entropy analysis (MSE)¹¹ is a useful tool for estimating the complexity of heartbeat fluctuations; and it can detect alterations in cardiac control with aging and predict clinical outcomes of patients with heart diseases^{10,12}. However, MSE results are not reliable when heartbeat signals consist of outliers^{13,14}. Thus, those data segments contaminated by outliers must be identified and excluded before performing MSE¹⁴. Such heavy-duty pre-processing is time consuming, thus compromising the clinical application of the analysis at the bedside. In addition, ignoring the segments with arrhythmia-related outliers may lead to loss of important information about the pathology of cardiac control. Therefore, there is an urgent need for the development of complexity analyses that can reliably quantify the degree of complexity in noisy physiological recordings with outliers.



In general, the change of a variable at a time point can be decomposed into two parts: the magnitude (absolute value) and the direction (sign)¹⁵. We hypothesize that dynamics in the sign time series can adequately reflect the complexity in raw data and that the complexity estimation based on the sign time series is more resilient to outliers as compared to raw data. Based on the hypothesis, we propose a new complexity analysis termed ‘multiscale symbolic entropy analysis’ (MSSE) that assesses the multiscale entropy of a signal from its sign time series. We also hypothesize that the

new method can reliably detect pathological alterations of cardiac control based on the complexity of heartbeat fluctuations even when the signals are contaminated by ectopic beats. To test these hypotheses, we conducted numeric simulations (and theoretical derivations) to examine the performance of the new method in signals with and without outliers. We also applied the method on human heartbeat recordings and examined whether complexity can be used detect the alterations of cardiac control in patients with congestive heart failure (CHF) and in critically ill patients with certain dysfunctional organ(s) and life continuation relying on a mechanical circulatory support system, namely, extracorporeal membrane oxygenator (ECMO) 16. Moreover, we compared the MSSE results with those of the traditional MSE.

2.2.2 METHODS

Multiscale entropy analysis

As described previously 11, MSE calculates the degree of irregularity in the fluctuations of a signal, $\{X_i\}$, at different time scales l . For each time scale, the time series is first coarse-grained to produce a new time series

$\left\{ Y_j = \frac{\sum_{i=n-l+1}^n X_i}{l} \right\}$, where $n = l \times j$. . Then the degree of irregularity in $\{Y_j\}$ is estimated using sample entropy (SpEn).

Multiscale symbolic entropy analysis

To better account for the influence of outliers, we propose a new algorithm, namely MultiScale Symbolic Entropy (MSSE) analysis. Different from MSE, MSSE considers the sign time series $\{b_j^l\}$ of each coarse-grained series at a time scale l . (Figure 3a), where b_j^l is either 1 when the corresponding y_i^l is increasing or 0 otherwise. To consider the quantization error in digital signals (e.g., 4 msec for signals with a sampling rate of 250 Hz), let $b_j^l = 0$ if the amplitude of a change is less than the quantization error. In addition, median values rather than mean values in non-overlapped windows are used to construct coarse-grained time series in order to minimize the impact of outliers (Figure S4).

To quantify the irregularity of a sign time series, the signal is first divided into sequences each with the same length m — the sequence length that is pre-selected (by default, $m = 8$ in this study). These m -bit sequences are divided into different categories based on their temporal patterns using the similar concept of the approximate/sample entropy²⁴. Specifically, a m -bit sequence is divided into multiple vectors, each consisting of D consecutive bits.

$\{(b_1, b_2 \dots b_D); (b_2, b_3 \dots b_{D+1}); \dots\}$, where D is the dimension of vectors. The number of paired vectors consisting of the exactly same binary codes is then obtained and is denoted as $n(D)$. The conditional probability of the sequence is determined by $n(D+1)/n(D)$. All sequences are assigned to different categories based on their conditional probabilities (i.e., sequences in a category have the same conditional probability). Categories are created using all possible m -bit sequences (not only the sequences present in a sign time series) and ranked based on the conditional probability, i.e., the conditional probability is the highest for the category with Rank =1 and lower for the categories with lower ranks (Figure 3). Then, based on the distribution of the sequences in different categories, the Shannon entropy $eSC(l)$ and the mean rank (namely, symbolic sample entropy) $eEC(l)$ can be obtained for the sign time series. Conceptually, eSC describes the information richness of a signal while eEC indicates the degree of uncertainty of the fluctuations.

Human heartbeat recordings

To test the performances of complexity analyses, we utilized existing heartbeat recordings of three groups of human subjects: (1) 46 control subjects at age of 65.9 ± 4.0 (SE) years old (24 hours); (2) 29 patients with congestive heart failure (CHF) at age of 55.2 ± 11.6 (SE) years old (24 hours); (3) 64 critically ill patients at age of 53.5 ± 18.2 (SE) years old who had severe dysfunction in certain organ(s) (i.e., fulminant myocarditis, severe respiratory failure, cardiogenic shock after cardiac surgery and septic shock)^{16,25,26} and relied on the extracorporeal membrane oxygenator (ECMO) to maintain life continuation (24 hours). Within the 64 ECMO patients, 33 survived while the others died.

The data of the first two groups are publically available in Physionet.org. The data of Group 3 were collected in the National Taiwan University (NTU) Hospital between March 2008 and March 2010. Patients were eligible for the present study if they were 18 years or older and had received ECMO for circulatory or respiratory failure that required mechanical support. The decision to use ECMO was made by experienced intensive care specialists or cardiac surgeons. The primary endpoint is death or urgent cardiac transplantation during the index admission. The patients were followed until discharge or death of the index admission. The Institutional Review Board of the NTUH approved the study and informed consent was obtained from each patient's next-of-kin in ECMO group and from each subject in control group in accordance with the NTU's human subject's research polices.

Surrogate data

We generated noise with different correlation properties by using a modified Fourier filtering method 27. The generated signals possess the desired power-law correlation functions that asymptotically behave as fractional Brownian motion (fBM) processes with different Hurst exponent (H) (see Supplementary I): white noise (Hurst exponent = 0.5), 1/f noise (Hurst exponent = 1), noise with stronger correlations (Hurst exponent = 1.2), and signals with anticorrelations (Hurst exponent = 0.4). For each type of noise, we generated 1000 signals each with 30,000 points.

Human heartbeat recordings with artificial ectopic beats are generated from total 24-hour heartbeat signals collected from 26 healthy young individuals. The signals have been previously reviewed and contain no abnormal beats (www.physionet.org\...). For each recording, two different ways were adopted to simulate the ectopic beats. We randomly selected certain percentage (e.g., 20% and 45%) of RR intervals and 1) replace the normal beats with intervals imitating premature ectopic beats [ref] of which the average RR was xx percent (XX~ XX in uniform distribution) of the mean value of the four normal hear beat intervals proceeding to these ectopic beats; or 2) replaced them with artificial outliers which is selected based on arrhythmia heartbeat intervals of the patients with CHF in Physionet database. In addition, we also consider the influence from the spike train, $\sum_i A_i \delta(t - \tau_i)$ which simulates the spurious peaks due to R wave detection errors []. Where A_i is the spike amplitude and τ_i is the temporal location of the spike. The spike trains were generated using a Bernoulli process of probability p

(e.g., 0.2 and 0.45). The output of the Bernoulli process was used to determine whether this sample should be added a spike. The sign of spike is also determined by Bernoulli process and the positive and negative spikes indicate the missing and false positive heart beat detection, respectively. In this study, the amplitude of each spike was assigned to be a normal distribution with mean value determined adaptively as half the median of 10 RR intervals adjacent to the spike location.

Autonomic filter

The certain automatic filtering procedure has been proposed in previous studies to address the time consuming procedure of manual filtering. For example, in each iteration, the recursive filtering procedure will remove the RR intervals that deviate from a predetermined tolerance determined adaptively by the ratio (1.25~0.75) of mean value derived from the preceding and following RR intervals(20 beats). A new RR interval derived from the linear interpolation of two adjacent normal beats will replace the removed one (see Figure 7).

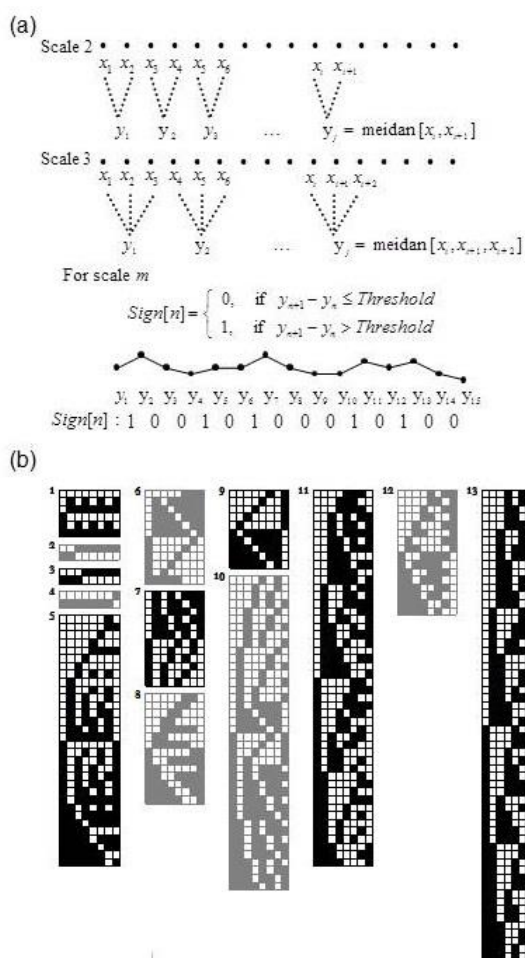
2.2.3 RESULTS

Assessment of complexity requires the examination of fluctuations at different time scales.

The theoretical concept behind the MSE and MSSE as well as many other complexity analyses is that the complexity of a time series cannot be reliably determined by statistical properties such as fluctuation amplitude and entropy at a fixed time scale because these properties can vary with time scale 11. To demonstrate this concept, we considered MSE results of (1) white noise that simply consists of uncorrelated data points, and (2) 1/f noise that is believed to represent the most complex fluctuation patterns in physical systems and is observed in many physiological systems under healthy conditions. As shown in Figure 2, the entropy value of a white noise can be smaller, equal to, or greater than that of a 1/f noise, depending on the time scale (and their standard deviations). Note that the entropy of a coarse-grained white noise at a time scale l is decreased by $\ln(l)/2$ while the entropy of a coarse-grained 1/f noise remains approximately constant at all different times scales (Figure 2 and Supplementary Material I). Thus, for the assessment of complexity, the entropy as the



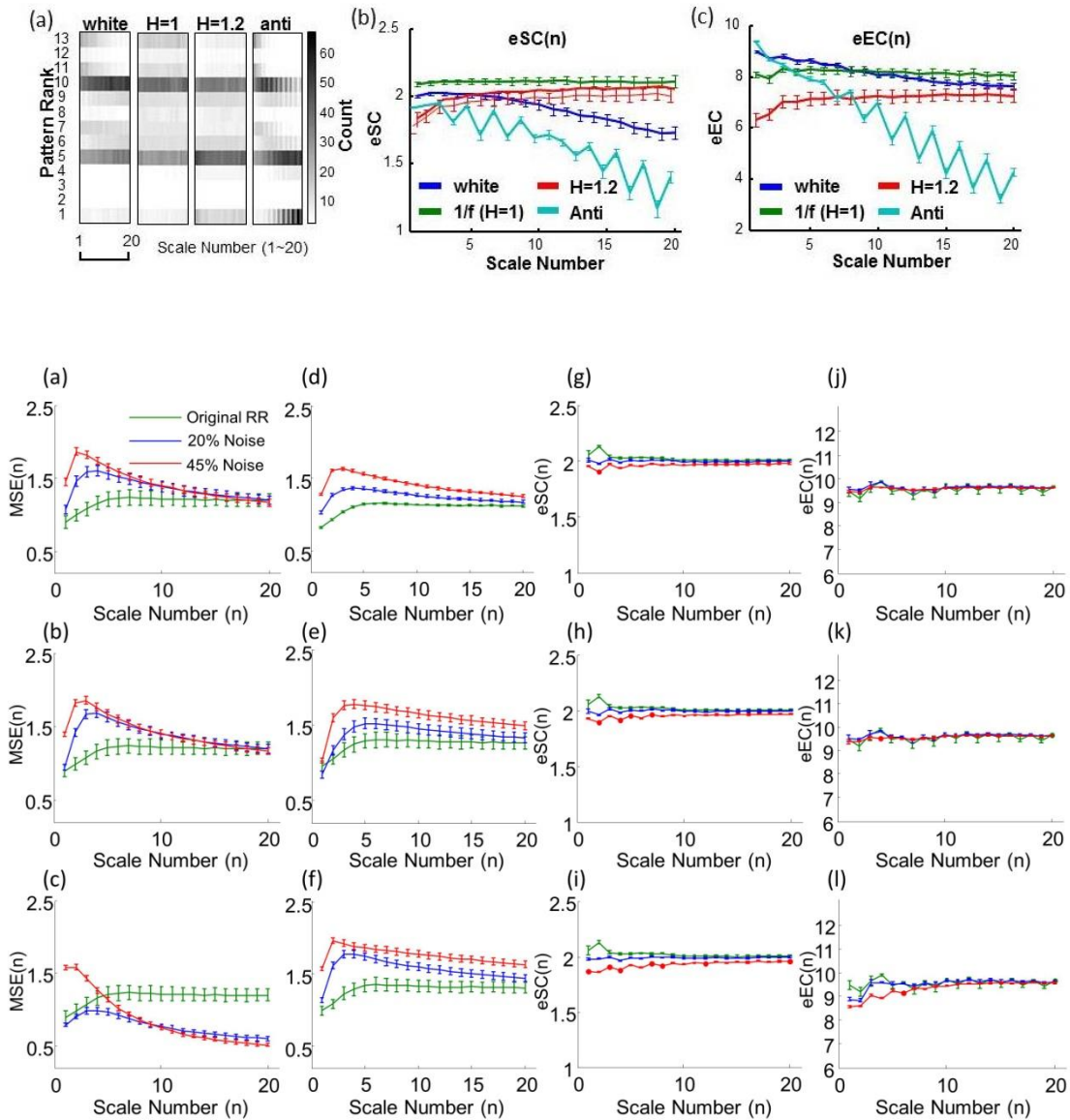
function of time scale (e.g., both the absolute values and the slope of the function) should be considered.



MSSE provides the similar information as MSE for signals without outliers.

To better account for the influence of outliers, we proposed a new algorithm, namely, multiscale symbolic entropy analysis, which quantifies entropies of fluctuations across different time scales (Figure 3 and see details in Methods). Figure 4a~c show the MSSE results for generated noise with different temporal correlations (see Methods). For all these signals, the two proposed MSSE measures (i.e., eSC and eEC) provided consistent results as the MSE measure does. For instance, eSC and eEC remained the same at different time scale for 1/f noise, decayed quickly at larger time scales for white noise, and decayed faster for anti-correlated noise. For noise with Hurst exponent >1 (stronger correlations as compare to 1/f noise), the entropy measures slightly increased with increasing time scales). Indeed both MSSE measures were highly correlated with the MSE measure at all time scales (Figure 5). We further applied MSE and MSSE to

heartbeat recordings of 26 healthy human individuals without outliers (Physionet: mean age: 31.7 ± 3.5 years old) (Figure 6). Consistent with previous findings [13], we found that all the entropy measures remained relatively constant at different time scales (except for very small time scales), suggesting fluctuation patterns similar to $1/f$ -noise (Figs. 6 a,g,i).



MSSE is more resilient to outliers

To examine how outliers impact the performances of MSE and MSSE, we generated surrogate data by randomly replacing some data points in the normal heartbeat intervals of those healthy subjects with three different type outliers due to the arrhythmic beats or

QRS detection error (Figure 7a~c and see details in Methods). The outliers significantly affected MSE, leading to overestimated entropies at time scales from 1-15 beats. The degree of overestimation depends on the time scales, i.e., more overestimation at smaller time scales. As a result, the MSE function became more like that of white noise (Figure 6a~c). The automatic filter can attenuate the effect of outliers in MSE, nevertheless the improvement is not yet satisfied (Figure 6d~f). In contrast, the results of MSSE remained virtually the same as those of the raw data, even when 45% artificial outliers were imposed (Figs. 6g~l).

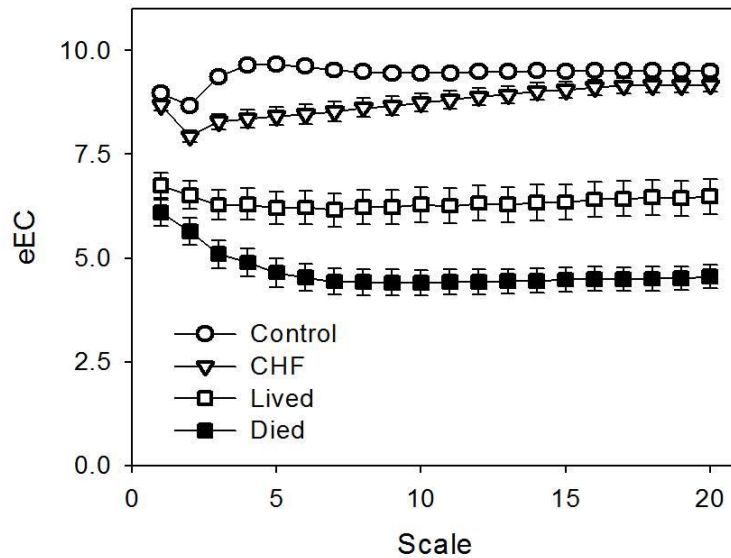
Complexity reveals altered cardiac dynamics in diseases

We next applied the MSSE and MSE to human heartbeat recordings of additional three groups: (1) 46 older control subjects; (2) 29 patients with congestive heart failure (CHF); and (3) 64 critically ill patients using ECMO. Unlike the data in healthy young subjects, heartbeat recordings of these three groups contained numerous abnormal/ectopic beats (Figure 1) such that many of them, especially those of ECMO patients, would be not usable if all ectopic beats must be removed. To test the performances of MSSE and MSE, we did not reject ectopic beats prior to performing the two analyses.

Overall there were significant group differences in all entropy measures. The differences between the control and CHF subjects were present exclusively at small time scales ($< \sim 5$ heartbeats). Specifically, the mean eEC at $< \sim 5$ beats showed a significant difference between the two groups (i.e., the CHF group has smaller eEC); and the slopes of MSE and eEC functions at $< \sim 5$ beats were consistently reduced in the CHF patients as compared to the controls (Table 1). In addition, the dependences of entropy measures on time scales in CHF patients behaved (Figure 8) more like that of correlated signals with $H > 1$ (Figs. 4b~c), e.g., the slope of eEC at scales 2-10 (0.084 ± 0.10) was larger than that of control subjects (0.048 ± 0.063 , $p < 0.05$). These results are consistent with the MSE results as reported previously^{10,11,13}, indicating reduced complexity in heartbeat fluctuations in CHF patients.

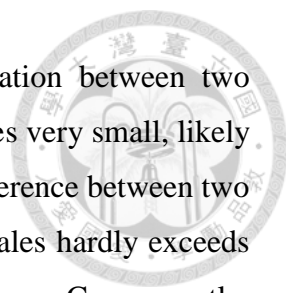
As compared to the controls, the ECMO patients had much lower values of MSSE measures at all time scales ($p < 0.0001$), suggesting significantly reduced heartbeat variability (see Table 1 and Figure 8). Similar to the controls, the ECMO patients also displayed a crossover in the MSSE functions (e.g., see the profile of eEC in Figure 8).

However, unlike the controls, the slope of eEC function at time scales below the crossover was negative in ECMO patients, resembling those observed in white noise or anti-correlated noise (Figs. 4b-c). These results suggest altered/disrupted cardiac control in these ECMO patients. Moreover, the changes of MSSE results in the ECMO group (i.e., reduced entropy values at all time scales and reduced slope at small time scales) were much more pronounced in those patients who died as compared to those who survived (see Table 1), suggesting more degraded cardiac control in the ECMO patients with fatal outcomes. At time scales >5 beats, eEC of ECMO survivors slightly increased with time scales (Figure 8), suggesting a behavior similar to fractional Brownian noise with Hurst exponent >1 .



Consistent with the MSSE results, the MSE function of ECMO patients also showed a negative slope at small time scales. But the slope was not different between the survived and the deceased patients (Table 1). The most unexpected results were that the MSE-derived entropy values of the ECMO patients, especially the survived patients, were close to or even larger than those of the controls at all time scales (see Table 1). This discrepancy is likely due to arrhythmia-related outliers in these signals that can significantly affect the performance of MSE, leading to artificial increases in entropy values as shown in the simulations (Figure 6a). Thus, the results of ECMO data provide further evidence for the limitation of MSE.

It should be noted that MSSE as well as the traditional MSE have the issue of

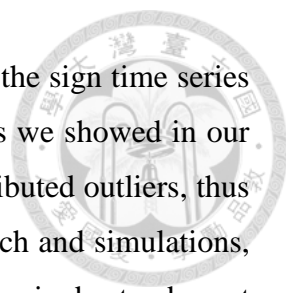


threshold effect (see the details in Supplementary III). The variation between two normal heartbeat intervals in the critically ill patients usually becomes very small, likely as a consequence of reduced autonomic nervous activity. Thus, the difference between two consecutive data points in the coarse-grained time series at large scales hardly exceeds the quantization error such that the sign series contain mainly zeros. Consequently, entropy measures are expected to become relatively stable at very large time scales, which was observed at scales >7 beats in ECMO patients (Figure S3).

2.2.4 DISCUSSION

With the emergence of the interdisciplinary field of nonlinear dynamics in medicine, how to extract health-related information in ECG-derived heartbeat fluctuations has attracted more and more attentions. It is hypothesized that complexity in heartbeat fluctuations reflects healthy cardiac control and reduced complexity in the fluctuations indicates degraded cardiac control as occurred with aging and under pathological conditions^{10,12,13,15}. Our results confirm this hypothesis and further show that cardiac complexity can predict survival of the critically ill patients who used ECMO to sustain their lives.

Complex heartbeat fluctuations is believed to stem from the interconnectedness of physiological mechanisms that is facilitated by a network of control nodes with feedback interactions¹. Such complexity is manifested by many nonlinear features, including strong correlations at multiple time scales^{17,18} that can be assessed by fractal analysis such as detrended fluctuation analysis (DFA) ¹⁹⁻²¹. Based on the estimation of randomness, multiscale entropy analyses such as MSE and MSSE also can be used to determine multiscale correlations by examining the relationship between entropy and time scale (Figs. 2, 4). For example, a negative slope of the entropy function indicates anti-correlated (i.e., simple oscillation, a repetitive pattern of an increase follow by a decrease) or uncorrelated fluctuations with the loss of feedback interactions¹³. Thus, the negative slope in the entropy function of the deceased ECMO patients suggests significantly reduced correlations in heartbeat fluctuations that are expectedly caused by the loss of feedback interactions in cardiac control of these patients. This finding provides evidence that reduced heartbeat correlations could predict the outcome of severely ill patients.



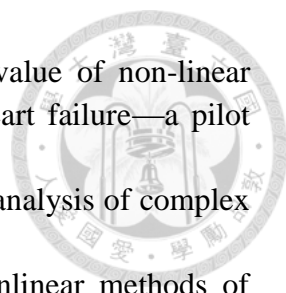
The proposed complexity analysis is based on the examination of the sign time series of a signal and its coarse-grained signals at different time scales. As we showed in our simulations, this approach can minimize the effect of randomly distributed outliers, thus helping to reveal the true dynamics in signals. Regarding the approach and simulations, there are a few points worth clarifying. First we note that ectopic beats do not necessarily occur randomly²². Thus, it is likely that the temporal distribution of ectopic beats in a real heartbeat signal may reflect certain aspects of cardiac control and/or pathological changes. More systemic studies are required to test how those ectopic beats contribute to complexity in heartbeat fluctuations. Second, by focusing on sign series, we do not imply that the magnitudes of a signal contain no useful information. Indeed the magnitude time series of a signal may contain dynamic information that is complementary to that in the sign series¹⁵. We sacrificed the possible useful information in the magnitude series because it can be easily contaminated by outliers. Finally, in MSSE, we proposed to use two entropy measures (i.e., eEC and eSC) to estimate the irregularity of the sign series at each time scale. Actually the MSSE results appear to be not sensitive to the method of estimating the irregularity, and similar results can be obtained using an alternative approach for the estimation of entropy in sign time series (see Supplementary Material II).

The number and severity of critically ill patients increase worldwide such that it is crucial for critical care professionals to make prudent and objective decisions on the allocation or termination of costly and risky treatments such as ECMO for these patients. Currently only about half of the adult patients receive ECMO²³. Due to the high cost of the treatment, it is important to identify patients who are likely to benefit from ECMO and to determine the appropriate timing of stopping ECMO. Physiology-based risk-classification tools are therefore needed to support decisions for or against continuous ECMO usage. Monitoring ECG is a routine procedure in clinical setting. Successfully applying the research findings of complexity in heartbeats to clinical practice (e.g., the use of ECMO) will have huge impacts on healthcare and medicine (e.g., ECMO usage). However, such a potentially important application has been impeded by the fact that, exclusively all previous complexity analyses require heartbeat signals without outliers or ectopic beats. This requirement is important because outliers can change significantly the estimated complexity based on the traditional complexity analyses such as MSE (Figure 6a). Removing outliers or ectopic beats is not trivial, not

only requiring specific expertise in ECG waveforms but also being very time-consuming. It has been shown that the recursive automatic filtering can help to minimize the effect of outliers on some heart rate variability measures such as frequency domain analysis[1]. However, how the automatic filtering affects complexity measures is not known. In addition, the procedure works well in the signals with the occasional and isolated ectopic beats but may not be applicable in the data with numerous and often continuous ectopic beats as occurred in ECG data of ECMO patients (see lower panel of Figure 7 in the revised manuscript). Thus, our results demonstrated the recursive automatic filtering only slightly attenuate the effect of outliers in MSE (Figure 6d~f). Moreover, ectopic beats in certain patients such as the ECMO patients occur so frequently that no continuous heartbeat recordings can be obtained after removing all ectopic beats. The proposed MSSE was specially designed to resolve these problems. With its reliability and high resilience to outliers, the method gives the hope of applying the theory of complexity in clinical practice. Further validation of the method using a large sample size is warranted.

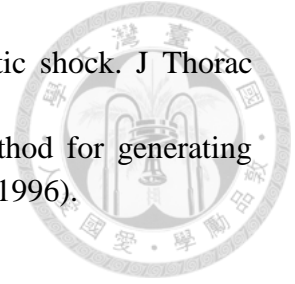
REFERENCES

1. Buchman, T. G. The community of the self. *Nature* 420, 246-251 (2002).
2. Goldberger, A. L. et al. Fractal dynamics in physiology: alterations with disease and aging. *Proc Natl Acad Sci* 99, 2466-2472 (2002).
3. Chen, Z., Ivanov, P. C., Hu, K. & Stanley, H. E. Effect of nonstationarities on detrended fluctuation analysis. *Phys Rev E* 65, 041107 (2002).
4. Hu, K., Ivanov, P. C., Chen, Z., Carpena, P. & Stanley, H. E. Effect of trends on detrended fluctuation analysis. *Phys Rev E* 64, 011114 (2001).
5. Huikuri, H. V. et al. Measurement of heart rate variability: a clinical tool or a research toy? *J Am Coll Cardiol* 34, 1878-1883 (1999).
6. Liang, W.-K. et al. Revealing the brain's adaptability and the transcranial direct current stimulation facilitating effect in inhibitory control by multiscale entropy. *NeuroImage* 90, 218-234 (2014).
7. Mäkikallio, T. H. et al. Fractal analysis of heart rate dynamics as a predictor of mortality in patients with depressed left ventricular function after acute myocardial infarction. *Am J Cardiol* 83, 836-839 (1999).
8. Ivanov, P. C. et al. Multifractality in human heartbeat dynamics. *Nature* 399, 461-465 (1999).
9. Ho, K. K. et al. Predicting survival in heart failure case and control subjects by use of fully automated methods for deriving nonlinear and conventional indices of heart rate dynamics. *Circulation* 96, 842-848 (1997).

- 
10. Ho, Y.-L., Lin, C., Lin, Y.-H. & Lo, M.-T. The prognostic value of non-linear analysis of heart rate variability in patients with congestive heart failure—a pilot study of multiscale entropy. *PloS one* 6, e18699 (2011).
 11. Costa, M., Goldberger, A. L. & Peng, C.-K. Multiscale entropy analysis of complex physiologic time series. *Phys Rev Lett* 89, 068102 (2002).
 12. Wessel, N., Malberg, H., Bauernschmitt, R. & Kurths, J. Nonlinear methods of cardiovascular physics and their clinical applicability. *Int J Bifurcat Chaos* 17, 3325-3371 (2007).
 13. Costa, M., Goldberger, A. L. & Peng, C.-K. Multiscale entropy analysis of biological signals. *Phys Rev E* 71, 021906 (2005).
 14. Voss, A., Schulz, S., Schroeder, R., Baumert, M. & Caminal, P. Methods derived from nonlinear dynamics for analysing heart rate variability. *Philos Trans R Soc London Ser A* 367, 277-296 (2009).
 15. Ashkenazy, Y. et al. Magnitude and sign correlations in heartbeat fluctuations. *Phys Rev Lett* 86, 1900 (2001).
 16. Chen, Y.-S. et al. Cardiopulmonary resuscitation with assisted extracorporeal life-support versus conventional cardiopulmonary resuscitation in adults with in-hospital cardiac arrest: an observational study and propensity analysis. *The Lancet* 372, 554-561 (2008).
 17. Goldberger, A. L. Non-linear dynamics for clinicians: chaos theory, fractals, and complexity at the bedside. *The Lancet* 347, 1312-1314 (1996).
 18. Goldberger, A. L. et al. Physiobank, physiotoolkit, and physionet components of a new research resource for complex physiologic signals. *Circulation* 101, e215-e220 (2000).
 19. Peng, C. K. et al. Non-equilibrium dynamics as an indispensable characteristic of a healthy biological system. *Integr Physiol Behav Sci* 29, 283-293 (1994).
 20. Peng, C. K. et al. Fractal mechanisms and heart rate dynamics. Long-range correlations and their breakdown with disease. *J Electrocardiol* 28 Suppl, 59-65 (1995).
 21. Hu, K., Van Someren, E. J., Shea, S. A. & Scheer, F. A. Reduction of scale invariance of activity fluctuations with aging and Alzheimer's disease: Involvement of the circadian pacemaker. *P Natl Acad Sci USA* 106, 2490-2494 (2009).
 22. Schulte-Frohlinde, V. et al. Complex patterns of abnormal heartbeats. *Phys rev E* 66, 031901 (2002).
 23. Mishra, V. et al. Cost of extracorporeal membrane oxygenation: evidence from the Rikshospitalet University Hospital, Oslo, Norway. *Eur J Cardio-Thorac Surg* 37, 339-342, doi:10.1016/j.ejcts.2009.06.059 (2010).
 24. Pincus, S. M. Approximate entropy as a measure of system complexity. *Proc Natl Acad Sci USA* 88, 2297-2301 (1991).
 25. Sun, H.-Y. et al. Infections occurring during extracorporeal membrane oxygenation use in adult patients. *J Thorac Cardiovasc Surg* 140, 1125-1132. e1122 (2010).
 26. Huang, C.-T., Tsai, Y.-J., Tsai, P.-R. & Ko, W.-J. Extracorporeal membrane

oxygenation resuscitation in adult patients with refractory septic shock. *J Thorac Cardiovasc Surg* 146, 1041-1046 (2013).

27. Makse, H. A., Havlin, S., Schwartz, M. & Stanley, H. E. Method for generating long-range correlations for large systems. *Phys Rev E* 53, 5445 (1996).





Chapter 3

Quantification of Attracting Orbit

3.1 New Method to Noninvasively Monitor Fetal Heart Rate during Cesarean Section

3.1.1 INTRODUCTION

Continuous fetal heart rate (FHR) monitoring is a routine for obtaining significant information about the fetal condition during labor. The intrapartum fetal ECG (FECG) has been shown capable of detecting newborn acidemia, and hypoxia [1]. However, the only clinically-available device for FECG analysis requires an invasive fetal scalp electrode, limiting its use to only those with ruptured membranes and a dilated cervix [2]. An alternative method, generally known as the non-invasive FECG, can monitor the FHR through the maternal ECG by placing electrodes on the mother's abdomen, and many researchers have developed signal processing methods to derive the FECG from the ECG recorded from the mother's abdomen [3-7]. However, to extract the FHR from the maternal abdominal ECG during cesarean section (CS) remains a challenge since the electrodes cannot be placed properly. The ECG electrodes could only be placed on the lateral sides of the maternal abdomen to avoid interfering with the surgical procedure that can significantly reduce the amplitude of FECG. Moreover, the CS procedure would introduce large motion artifacts and myopotential interference which are difficult to deal with by using traditional methods proposed to extract FECG recorded in the resting state during the prenatal examination. For example, methods based on independent Component Analysis (ICA) might fail since the assumption-the sources (mother and fetal ECGs) are mutually statistically independent-might not be true in the long-term recording for the CS delivery. Also, the frequent position changes of the fetus position during CS delivery can cause the morphological variation of FECG and reconstruction of FECG by the wavelet method with a single selected base (mother wavelet) might be unreliable.

In the present study, we develop a method to derive the FECG by adaptively

suppressing the maternal ECG and other interferences from the maternal abdominal ECG. Since the fetal status could not be properly monitored during the CS delivery, it is of clinical importance to monitor FHR during the procedure especially for early identification of fetal distress. Our goal of the present study is to use the novel method to derive FHR noninvasively from the maternal abdominal ECG during CS.

3.1.2 MATERIALS AND METHODS

Subjects scheduled for elective cesarean delivery from September 2012 to December 2012 were included in the study. Subjects admitted for CS were asked if they were willing to join the study when receiving pre-operative anesthesia assessment. Informed consent was obtained one day before in CS after detailed explanation of the study procedure. Only subjects with uncomplicated pregnancies and excluded those with pregnancy-induced hypertension and gestational diabetes were included.

After the parturient were transferred into the National Taiwan University Hospital operating room, they were placed in a supine position, equipped with standard monitor, a non-invasive blood pressure cuff, and a pulse oximeter. The ECG signals were obtained from five abdomen electrodes (four electrodes for signal collecting and one for reference) placed away from the surgical site and recorded using a PC-based EEG system (Neuron-Spectrum-4, Neurosoft Company, Russia) in 16 bit, 2 KHz sampling format (see Figure 1).

After being prehydrated with 1000ml lactated Ringer's solution, the parturient was turned on her side. A 27-gauge Quincke spinal needle was introduced into the subarachnoid space at the L2-3 or L3-4 interspace in the lateral decubitus position, and 10-12 mg of 0.5% hyperbaric bupivacaine was administered to achieve sensory anesthesia (determined by pin prick) extending to the T4 dermatome. Hypotension was treated immediately by intravenous injection of 4-8 mg ephedrine in repeated doses. Other medications were avoided because of their potential influence on measurements. The recordings were performed in the operating room during three different processes: preparing for operation, 5 minutes after spinal anesthesia and 5 minutes before cesarean delivery.

In the study, we included four electrodes with one reference ground. The reference

ground was used to serve as a potential reference against which other potentials can be measured and limit the build-up of static electricity, while the other four electrodes were used to do the QRS detection as well as the analysis; since the fetal positions are changing during the laboring process, it is our experience that we can ensure the detection of high quality signals (at least one of the voltage signals) by using the applied experimental setting. After that, we could select the highest quality results for analyzing. The ECGs were recorded during the surgery, and the analyses stated below were performed off-line without any interference to the surgery.

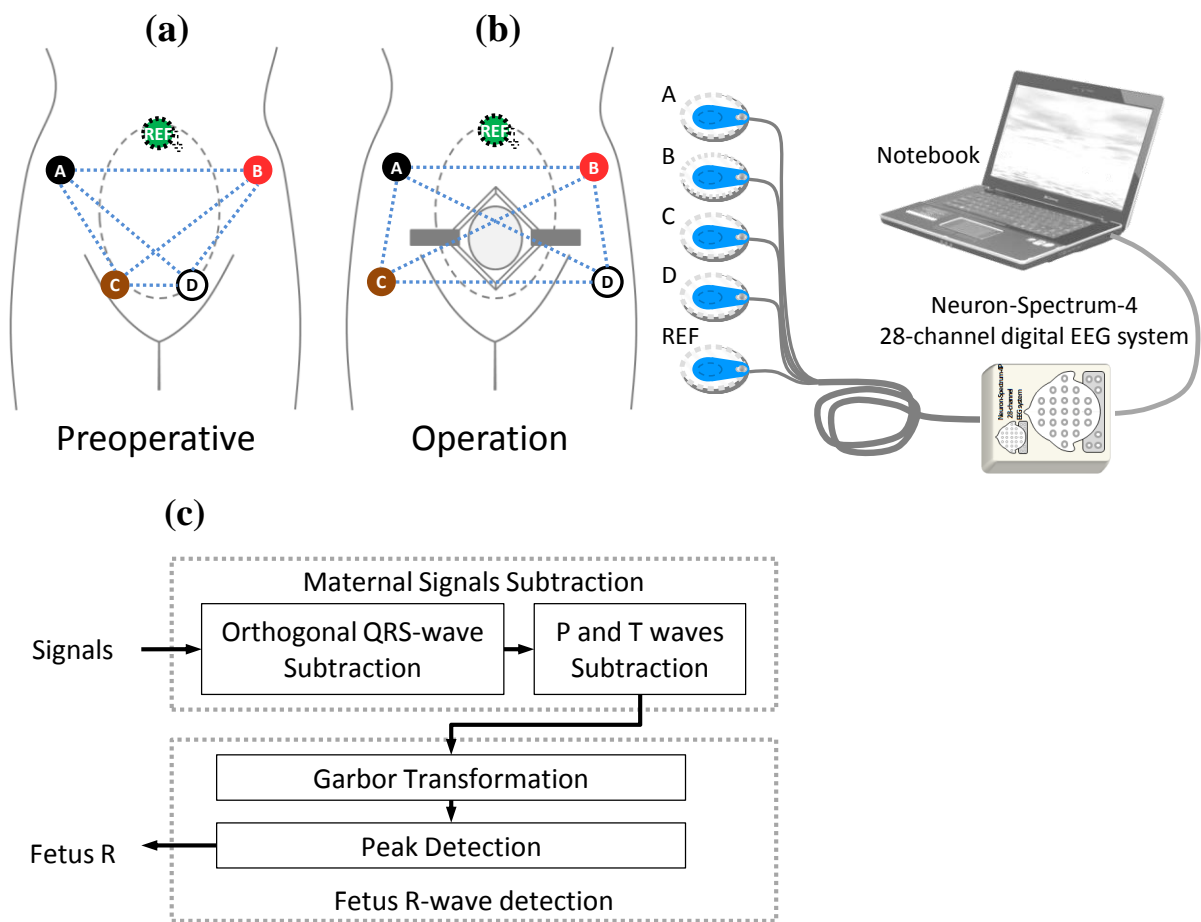
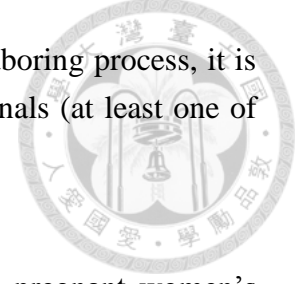


Figure 1. Five abdomen electrodes (four electrodes for signal collecting and one for reference) were placed in different ways for two scenarios: (a) before and (b) during the surgical operations. (c) The work-flow chart of our proposed algorithm. We use four electrodes (marked as A, B, C, and D) for signal acquisition and one (marked as G) for common system reference electrode. Since an voltage signal usually represents a difference between the voltages at two electrodes in EEG measurements, the number of voltage signals in our study would be six (two out of four leads: V_{AB} , V_{AC} , V_{AD} , V_{BC} ,

V_{BD} , V_{CD}). Noted that the fetal positions are changing during the laboring process, it is our experience that we can ensure the detection of high quality signals (at least one of the voltage signals) by using the applied experimental setting.



Maternal QRS-T cancellation

The FECG is derived from cutaneous electrodes placed on the pregnant women's abdomen. The FECGs are very weak and usually overwhelmed by the maternal ECG, so the maternal ECG need to be first removed to make way for fetal heart beat detection. Ideally, many studies have proposed to reconstruct the FECG signal by 1) identifying each maternal beat, 2) creating a template acquired from the average of those maternal beats to filter out the blended fetal heart beats and 3) finally subtracting the template from each maternal beat [8, 9]. However, since the waveforms of the maternal ECG are not consistent in different heart beats, this limits effective performance (i.e., the subtraction of the fixed template from an inconsistent maternal ECG will produce a large residue intermittently to severely disturb fetal heart beat detection). An adaptive template therefore was proposed in this study to substantially suppress the material residue. Figure 2 shows the illustrative maternal ECG signals processed by the proposed algorithm step by step. Briefly, the maternal heart beats were firstly identified and the i th maternal QRS wave was denoted as:

$$QRS_i(t) = x(t) \cdot e^{-c \left(\frac{t - \tau_i}{W} \right)^2} \quad (1)$$

Where $x(t)$ is the ECG signals obtained from abdomen electrodes, τ_i is maternal R wave peak time, and W is width of the QRS complex. Then a QRS-template, $\hat{QRS}(t)$ was created by averaging the maternal QRS waves with Gaussian weighting function, $G(t)$.

$$\hat{QRS}(t) = \frac{1}{L} \sum_{i=1}^L [QRS_i(t) \otimes \delta(t + \tau_i)] \cdot G(t) \quad (2)$$

Then, Hilbert transform is applied to the resultant QRS-template to generate another basis, $H(\hat{QRS})(t)$ which is mathematically orthogonal to the QRS-template (see lower panel, Figure 2a) [10, 11].

Respiration and body movements usually cause inconsistent geometrical projection of the depolarization loop onto the electrodes. The adaptive combination of these two orthogonal bases can accommodate the template to the nonstationary change of

maternal QRS waveform induced by inconsistent geometrical projection, i.e.,

$$dQRS_i(t) = \frac{\int QRS_i(t) \otimes \delta(t + \tau_i) \cdot \hat{QRS}(t)}{\left| \int \hat{QRS}(t) \right|^2} \hat{QRS}(t) + \frac{\int QRS_i(t) \otimes \delta(t + \tau_i) \cdot H(\hat{QRS})(t)}{\left| \int H(\hat{QRS})(t) \right|^2} H(\hat{QRS})(t) \quad (3)$$

as shown in Figure 2(a), removing such adaptive templates from the ECG recordings can suppress the maternal QRS complex substantially,

$$x_{dQRS}(t) = x(t) - \sum_{i=1}^L dQRS_i(t) \otimes \delta(t - \tau_i) \quad (4)$$

In some situations, the maternal P and T waves still appear in the residues even after the QRS complex has been perfectly removed (Figure 2b). Nevertheless, the P and T waves both occupy the low frequency band in the spectrum and are insensitive to body movements. Therefore, the subtraction of the P and T waves can be simply implemented by removing the average of all P-T segments (see Figures 2b-c).

$$x_f(t) = x_{dQRS}(t) - \sum_{i=1}^L dPQRST_i(t) \otimes \delta(t - \tau_i) \quad (5)$$

$$dPQRST_i(t) = \frac{1}{L} \sum_{i=1}^L \left[x_{dQRS}(t) \cdot \text{rect}\left(\frac{t - \tau_i}{W_{PT}}\right) \right] \otimes \delta(t + \tau_i)$$

, where W_{PT} is the PT interval.

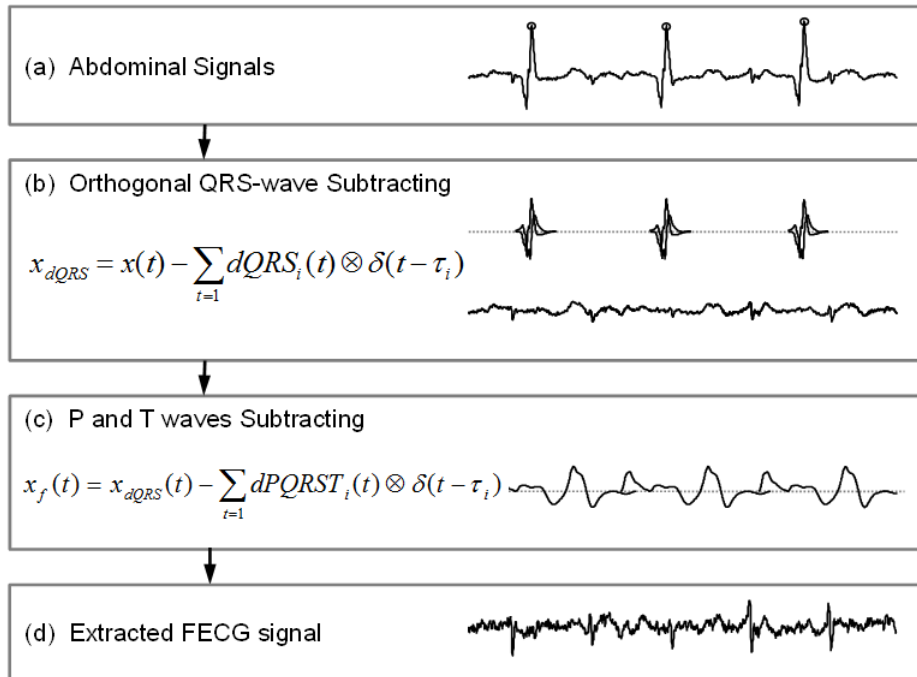
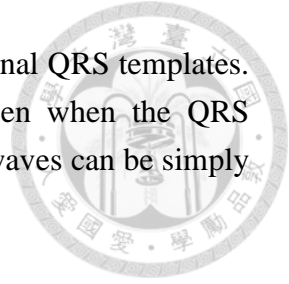


Figure 2. (a) An example of raw data with maternal ECG interferences which could be

suppressed significantly by the adaptive combination of two orthogonal QRS templates. (b) The maternal P and T waves still appear in the residues even when the QRS complexes are completely removed. (c) The subtraction of P and T waves can be simply implemented by removing the average of all P-T segments.



We apply the Gabor transform to build the time-frequency representation of the reconstructed FECG signals, $x_f(t)$ shown in Figure 3. Apparently, after P-QRS-T cancellation, the fetal heart beats occupy the frequency range of ~10Hz to 20Hz intermittently and exhibit less contamination. Therefore, the fetal QRS waves can be identified by an easy criterion: whether the integrated power within the adaptively selected frequency band crosses the threshold.

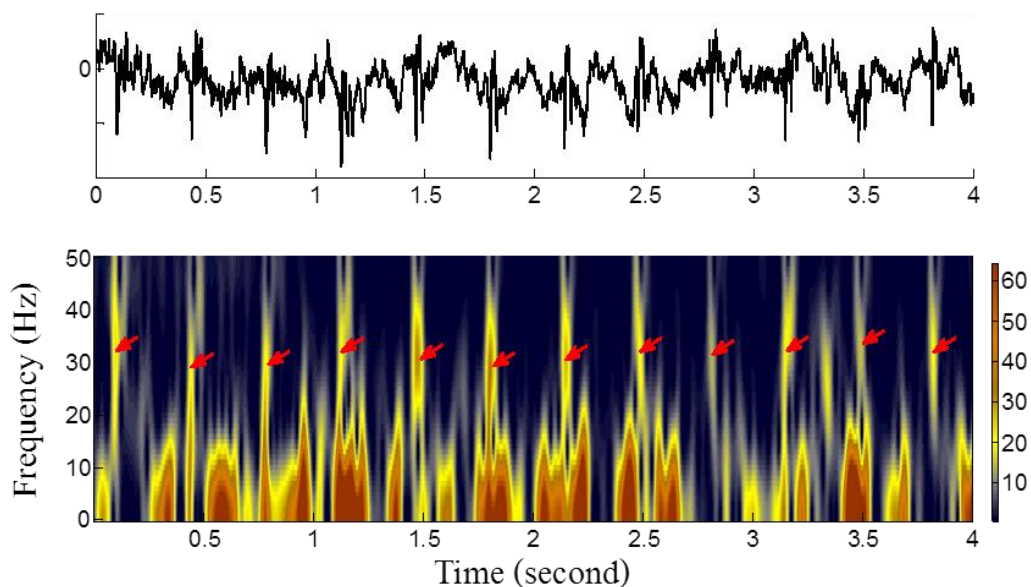
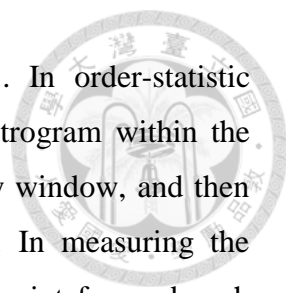


Figure 3. An example of Gabor time frequency representation (lower panel) of ECG signals with suppressed maternal ECG (upper panel). The red arrows indicate the location of the fetal QRS waves, which occupy a frequency range of ~10Hz to 20Hz intermittently that are free of maternal contamination in Gabor representation.

The fetal heart beats were detected generally by threshold crossing. To account for variability in waveform amplitude, we set an adaptive threshold on the integrated power within the adaptively selected frequency band. A nonlinear strategy, namely order-statistic filter, was used as the most crucial step to determine the adaptive threshold. The concept of order-statistic filtering was adapted using median filtering



algorithm, which is commonly used in imaging denoising [12]. In order-statistic filtering, the input data (i.e., the integration of Gabor power spectrogram within the adaptively selected band) were simply weighted with sliding Tukey window, and then the maximum among the weighted data was obtained as output. In measuring the envelope with order-statistic filtering, the window was shifting 1-point forward each time until the entire set of signals was analyzed, and the procedure was repeated for each windowed data, the fetal heart beat peaks were determined by finding the points with equal magnitude to the integration of Gabor power spectrogram within the adaptively selected band and its envelope. The method basically can reject the pseudo peaks which may be caused by electromyogram or maternal heart beat residue between two consecutive fetal heart beats [13].

To provided evidence to explain the veracity of FECG detection results, we applied our proposed “Fetal QRS Detection” method to the experimental signals download from “Non-Invasive Fetal Electrocardiogram Database” of “PhysioBank” (A valid open-source online database; <http://physionet.nlm.nih.gov/pn3/nifecgdb/>), and the accurate detection rate is higher than 95%.

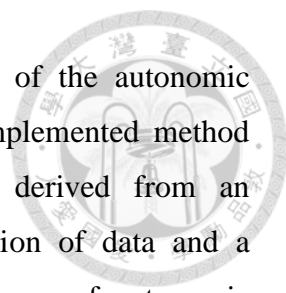
Fetal Heart Rate Variation

Linear time-domain parameters

The linear time-domain parameters including mean heart rate, standard deviation of normal-to-normal intervals (SDNN), maximum and minimum heart rate at different stages of the baseline, both 5 minutes after anesthesia, and 5 minutes before CS delivery, were computed. Ectopic beats were inspected visually and rejected by comparison with the adjacent QRS morphologic features. For each stage, the annotated signals of the 90-second ECG recording, which consisted of more than 95% of qualified normal sinus beats, were then used for analysis of HRV. After the outliers of FHR were rejected, we evaluated the mean value of its highest quarter as the mean maximum FHR, and represent the mean value of the lowest quarter as the mean minimum FHR.

Poincaré method to assess the autonomic function

Unlike the well-established link between the density of the spectrum in specific bands and autonomic system of the adult, the frequency domain analysis of the FHR variation is still too preliminary to show utility. Therefore, instead of frequency domain



parameters, the Poincaré method was applied to the assessment of the autonomic nervous function [14-16]. Poincaré plot is a simple and easily implemented method which is capable of summarizing an entire RR time series derived from an electrocardiogram in the picture to provide 'real time' visualization of data and a quantitative technique which gives information on nonlinear features of autonomic system [17]. Its clinical ability as a predictor of disease and cardiac dysfunction has been proven [18] thus is becoming a popular technique in the field of HRV. The current study attempted to apply this method to the assessment of fetal autonomic nervous activities in different stages. The Poincaré plot is a two dimensional scatter distribution, which is constructed by plotting each RR interval against the previous one. Qualitative analysis of the Poincaré plot was proposed by fitting an ellipse to the shape of the plot. The fast beat-to-beat variability (SD1) determined by the dispersion along the minor axis of the ellipse is characterized as a marker of parasympathetic modulation, while the long term beat-to-beat variability (SD2) determined by the dispersion along the major axis of the ellipse is usually characterized as a marker of parasympathetic and sympathetic modulation. The reduced SD1/SD2 ratio may be used as indicative of the increase in the sympathetic modulation.

Symbolic Dynamics of HRV

Guzzetti et al. have proposed a nonlinear method of HRV analysis (symbolic dynamic analysis) to quantify the predominance of sympathetic or parasympathetic cardiac modulation in conditions while the use of a linear HRV approach is limited or disputed [19]. The full range of the sequences was divided into 6 levels (from 0 to 5) based on a simple criterion that the 6 levels are equally spaced within the maximum and minimum RR intervals. The symbolic sequences were sorted into categories, and the sequence length L was 3. [19]. All possible patterns were classified into 3 categories: (1) patterns with no variation (0 V; all 3 symbols were at the same level); (2) patterns with 1 variation (1 V; 2 consecutive equal-leveled symbols with one at different level); and (3) patterns with 2 variations (2 V; all symbols were at different levels compared to the previous one). The percentage of the patterns 0 V, 1 V, and 2 V were calculated (see Table 1).

Statistical Analysis

The average values were expressed as mean \pm SD. The normal distribution of the data

was first tested using the Shapiro–Wilk test before the subsequent statistical analysis of the computational parameters. The serial data baseline, 5 minutes after anesthesia, and 5 minutes before CS delivery, were then compared by repeated measures analysis of variance. If the result demonstrated a significant time-related effect, either paired Student’s t test or Tukey HSD with Bonferroni correction were performed for the comparisons between groups. The Statistical Package for the Social Sciences (SPSS, version 16.0 for Windows. SPSS Inc., Chicago, IL) was used for all statistical analyses. A P value of less than 0.05 was considered statistically significant.

3.1.3 RESULTS

Subject characteristics and procedures

A total of 17 parturients scheduled for elective cesarean delivery were included after their written informed consent was obtained. The parturient age was 35.1 ± 3.9 years. The gestational age was 38.7 ± 0.5 weeks. The body weight of the fetus was 3100.8 ± 192.9 g. The Apgar score changed from 8.6 ± 0.7 to 9.8 ± 0.4 1 minute and 5 minutes after delivery respectively. During the study, no complications were noted.

Table 1. Temporal evolutionary changes of time domain HRV parameters and autonomic nervous function measures (Poincaré method) for Baseline (preparing for operation), 5 minutes after anesthesia and 5 minutes before caesarean-section delivery.

	Baseline	5 minutes after anesthesia	5 minutes before caesarean-section delivery
Min HR (per minute)	131.36±6.03	133.75±8.64	142.79±15.71 ⁺
Max HR (per minute)	141.24±7.81	151.16±7.75 [*]	163.68±14.06 ⁺⁺
Mean HR (per minute)	135.88±6.26	141.86±7.69 [*]	153.33±14.51 ⁺
SDNN (ms)	13.01±6.89	21.30±9.05 ^{**}	22.88±12.01 ⁺
SD1	7.86±4.42	9.75±6.01	9.03±8.06
SD2	16.18±10.01	27.92±12.28 ^{**}	30.54±15.88 ⁺
SD1/SD2	0.65±0.41	0.38±0.18 [*]	0.33±0.24 ⁺
0V	0.30±0.13	0.37±0.14	0.39±0.14 ⁺
1V	0.37±0.06	0.34±0.05	0.36±0.06
2V	0.33±0.10	0.29±0.12	0.25±0.10 ⁺

Min HR, minimum heart rate; Max HR, maximum heart rate; Mean HR, mean

normal-to-normal intervals; SDNN, standard deviation of normal-to-normal intervals; SD1, fast beat-to-beat variability; SD2, the long term beat-to-beat variability; SD1/SD2, the ratio of SD1 to SD2; 0V, patterns with no variation; 1V, patterns with 1 variation; 2V, patterns with 2 variation; *P < 0.05 baseline vs. 5 minutes after anesthesia; ** P < 0.001 baseline vs. 5 minutes after anesthesia; +P < 0.05 baseline vs. 5 minutes before caesarean-section delivery.; ++P < 0.001 baseline vs. 5 minutes before caesarean-section delivery.

Temporal evolutionary changes of heart rate variability of fetus during delivery

Post hoc pairwise comparisons of HRV parameters against baseline values were shown in Table 1. The mean minimum FHR 5 minutes after anesthesia was similar to the baseline FHR (133.75 ± 8.64 vs. 131.36 ± 6.03 per minute, $P > 0.05$) but increased significantly before delivery (142.79 ± 15.71 vs. 131.36 ± 6.03 per minute, $P < 0.05$). As for the mean maximum FHR and the mean FHR, both increased significantly 5 minutes after anesthesia and 5 minutes before delivery as compared with those of the baseline stage. As for the HRV parameters, the SDNN increased both 5 minutes after anesthesia and 5 minutes before delivery (21.30 ± 9.05 vs. 13.01 ± 6.89 , $P < 0.001$ and 22.88 ± 12.01 vs. 13.01 ± 6.89 , $P < 0.05$). The SD1 did not change during anesthesia, while the SD2 increased significantly both 5 minutes after anesthesia (27.92 ± 12.28 vs. 16.18 ± 10.01 , $P < 0.001$) and 5 minutes before delivery (30.54 ± 15.88 vs. 16.18 ± 10.01 , $P < 0.05$) stages. The SD1/SD2 ratio decreased significantly both 5 minutes after anesthesia (0.38 ± 0.18 vs. 0.65 ± 0.41 , $P < 0.05$) and 5 minutes before delivery (0.33 ± 0.24 vs. 0.65 ± 0.41 , $P < 0.05$) stages. For the result of symbolic dynamic analysis, the percentage of 0 V was significantly higher in 5 minutes after anesthesia (0.30 ± 0.13 vs. 0.39 ± 0.14 , $P < 0.05$); on the contrary, the percentage of 2 V was also significantly reduced in 5 minutes after anesthesia (0.33 ± 0.10 vs. 0.25 ± 0.10 , $P < 0.05$); while 0V and 2V percentages did not change during anesthesia.

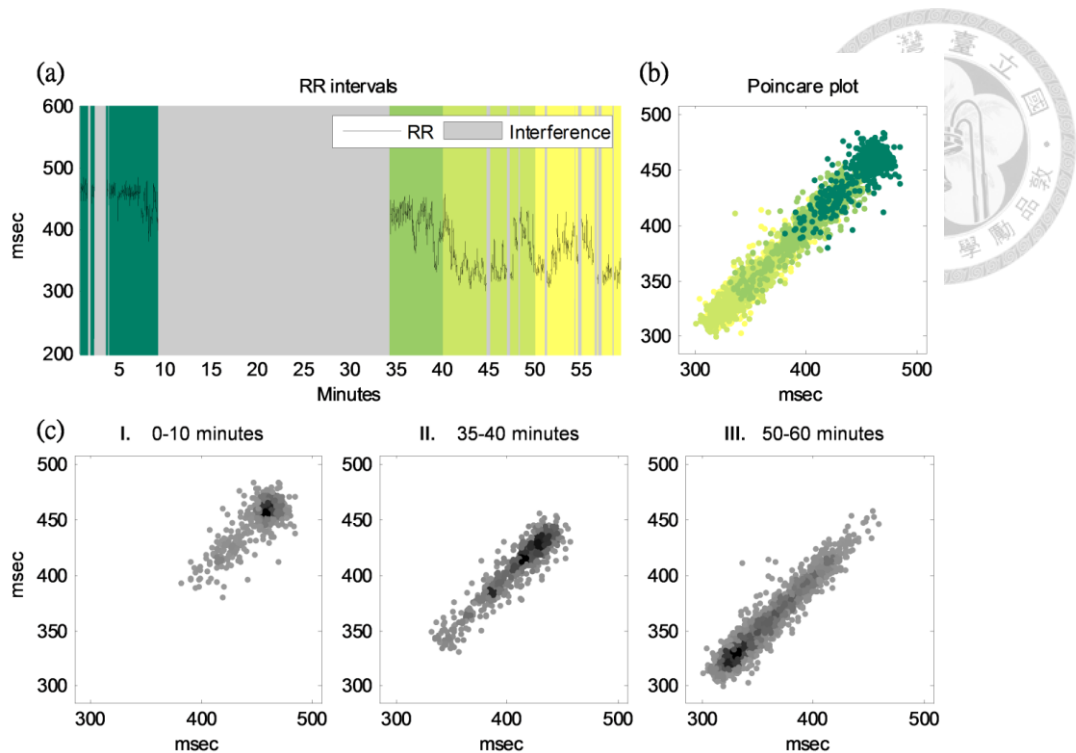


Figure 4. (a) Fetal R-R interval time series of a study subject from baseline preparation to the caesarean-section delivery of the fetus. Three time points—baseline, 5 minutes after anesthesia, and 5 minutes before delivery—were marked by colors of deep green, light green, and yellow. The Poincaré plot for the whole recording is marked with different colors to show the temporal change (b). Detailed Poincaré plot of three stages is provided in Figure 4c to 4e.

Figure 4a illustrates the fetal R-R interval time series of a study subject from baseline preparation to the caesarean-section delivery of the fetus. Three time points: baseline, 5 minutes after anesthesia, and 5 minutes before delivery were marked by colors of deep green, light green, and yellow. The corresponding scatter distribution of each RR interval against the previous one for the whole recording are plotted with different colors to show the temporal change (see Figure 4b). We also provide the detailed Poincaré plot of the three stages in Figure 4c to 4e. Obviously, both long term beat-to-beat variability (SD2) and mean heart rate showed an increased trend as time evolved.

3.1.4 DISCUSSION

The Maternal abdominal ECG has been successfully applied to the monitoring of FHR clinically [2-7]. However, to monitor FHR using maternal abdominal ECG during CS is more challenging, since the ECG pads could not be placed in the usual locations leading to low FECG signals. In the current study, we developed a robust method to

adaptively subtract maternal ECG and successfully derived FHR from a noisy composite ECG during CS. This method potentially could be applied to monitoring FHR clinically.

A considerable advantage of our method for this composite signal is that, in our algorithm, the maternal QRS template is not fixed but is adaptive. Since the ECG signal is nonstationary and is subject to many sources of interference, our algorithm overcomes the difficulty by generating an orthogonal basis of the QRS template through Hilbert transformation. The adaptive combination of these two orthogonal bases can accommodate the template to the nonstationary change of maternal QRS waveform induced by inconsistent geometrical projection. Through this approach, the maternal ECG could be substantially subtracted in a real-time and adaptive manner. As for the other application of our proposed method, since the atrial activity is uncoupled to ventricular activity during AF, it is also appropriate to apply our proposed method to extract the atrial signal by removing the QRS waveform using the ECGs recorded from the patients who suffered from the atrial fibrillation (AF) [20].

Tulppo et al [17] fitted an ellipse to the shape of the Poincaré plot and defined two standard descriptors of the plot, SD1 and SD2, for quantification of the Poincaré plot geometry. These standard descriptors represent the minor axis and the major axis of the ellipse respectively. SD1 (short term variability) is an indirect measure of parasympathetic activity, while SD2 (long term variability) is more strongly related to sympathetic activity than parasympathetic activity [25]. The symbolic dynamic analysis proposed by Guzzetti et al. [19] can be one alternative to quantify the prevalence of sympathetic or parasympathetic cardiac modulation in conditions while the use of a linear HRV approach is limited or disputed. An increase in sympathetic activity results in an increase in the percentage of V_0 [19]. Our results showed that the percentage V_0 was significantly higher 5 minutes before delivery as compared with that in baseline stage. Our study showed that during CS, the SD1 of FHR remained similar while the percentage of SD2 and V_0 increased together with increasing FHR, indicating that the sympathetic nerve is activated during anesthesia.

The FHR is controlled by the autonomic nervous system. The inhibitory influence on the heart rate is conveyed by the vagus nerve, whereas excitatory influence is conveyed by the sympathetic nervous system [26]. Stimulations of the peripheral nerves of the fetus by its own activity (such as movement) or by uterine contractions cause

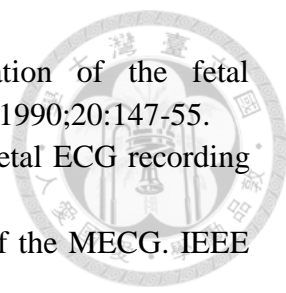
acceleration of the FHR [26]. Studies have demonstrated that abnormal FHR during spinal or epidural anesthesia are primarily the results of uterine hypertonus and maternal hypotension [27, 28]. In the current study, the FHR was significantly increased but remained within the normal range, which might be attributed to vasodilatation caused by spinal anesthesia.

There are several potential limitations of the study. First, the study population was small. The effective data are difficult to obtain because of the high possibility of contamination and interference during the delivery; nevertheless, we try recording three additional electrodes simultaneously in order to minimize the weak points. Second, we did not validate our algorithm by invasive fetal scalp ECG. Third, no fetal events occurred during the study. A larger population study could validate the meaning of the derived parameters.

In conclusion, we developed a novel method to automatically derive the FHR from the maternal abdominal ECG and proved that it is feasible in the challenging clinical setting of the cesarean section.

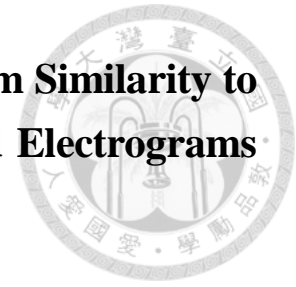
REFERENCES

1. Amer-Wahlin I, Bördahl P, Eikeland T, Hellsten C, Norén H, Sörnes T, Rosén KG: ST analysis of the fetal electrocardiogram during labor: Nordic observational multicenter study. *J Matern Fetal Neonatal Med* 2002;12:260–6.
2. Clifford G, Sameni R, Ward J, Robinson J, Wolfberg AJ: Clinically accurate fetal ECG parameters acquired from maternal abdominal sensors. *Am J Obstet Gynecol* 2011;205:47.e1-5.
3. Wu S, Shen Y, Zhou Z, Lin L, Zeng Y, Gao X: Research of fetal ECG extraction using wavelet analysis and adaptive filtering. *Comput Biol Med* 2013;43:1622-7.
4. Evaggelos C, Markos G, Dimitrios I Fotiadis: Detection of fetal heart rate through 3-D phase space analysis from multivariate abdominal recordings. *IEEE Trans Biomed Eng* 2009;56:1394-406.
5. Ibahimy MI, Ahmed F, Mohd Ali MA, Zahedi E: Real Time signal processing for fetal heart rate monitoring. *IEEE Med Biol Eng Comput* 2003;50:258–62.
6. Kotas, M: Projective filtering of time-aligned beats for foetal ECG extraction. *Bull Pol Ac Tech* 2007;55:331–9.
7. Kanjilal PP, Saha G: Fetal ECG extraction from single-channel maternal ECG using singular value decomposition. *IEEE Trans Biomed Eng* 1997;44:51-9.

- 
8. Abboud S, Barkai G, Mashiach S, Sadeh D: Quantification of the fetal electrocardiogram using averaging technique. *Comput Biol Med* 1990;20:147-55.
 9. Abboud S, Alaluf A, Einav S, Sadeh D: Real-time abdominal fetal ECG recording using a hardware correlator. *Comput Biol Med* 1992;22:325-35.
 10. Bergveld P, Meijer WJ: A new technique for the suppression of the MECG. *IEEE Trans Biomed Eng* 1981;28:348-54.
 11. Selesnick IW: Hilbert transform pairs of wavelet bases. *IEEE Signal Proc Let* 2001;8:170-3.
 12. Cheng F, Venetsanopoulos AN: An adaptive morphological filter for image processing. *IEEE Trans Image Process* 1992; 1:533-539.
 13. Chang YC, Lo MT: Methods for processing sequential data to identify possible peak points and to estimate peak to noise ratio of sequential data. U.S. Patent Application 13/682,757.
 14. Karmakar CK, Khandoker AH, Voss A, Palaniswami M: Sensitivity of temporal heart rate variability in Poincaré plot to changes in parasympathetic nervous system activity. *Biomed Eng Online* 2011;10:17-30.
 15. Lerma C, Infante O, Pérez-Grovas H, José MV: Poincaré plot indexes of heart rate variability capture dynamic adaptations after haemodialysis in chronic renal failure patients. *Clin Physiol Funct Imaging* 2003;23:72-80.
 16. Stein PK, Domitrovich PP, Hui N, Rautaharju P, Gottdiener J: Sometimes higher heart rate variability is not better heart rate variability: results of graphical and nonlinear analyses. *J Cardiovasc Electrophysiol* 2005;16:954-9.
 17. Tulppo MP, Mäkikallio TH, Takala TE, Seppänen T, Huikuri HV: Quantitative beat-to-beat analysis of heart rate dynamics during exercise. *Am J Physiol.* 1996;271:H244-252.
 18. Kamen PW: Heart rate variability. *Aust. Family Physician* 1996;25:1087–1094.
 19. Guzzetti S, Borroni E, Garbelli PE, Ceriani E, Della Bella P, Montano N, Cogliati C, Somers VK, Malliani A, Porta: Symbolic dynamics of heart rate variability: a probe to investigate cardiac autonomic modulation. *Circulation* 2005; 112: 465–470.
 20. astells F, Mora C, Rieta JJ, Moratal-Perez D, Millet J: Estimation of atrial fibrillatory wave from single-lead atrial fibrillation electrocardiograms using principal component analysis concepts. *Medical and Biological Engineering and Computing* 2005; 43:557-560.
 21. Kamen PW, Krum H, Tonkin AM: Poincaré plot of heart rate variability allows quantitative display of parasympathetic nervous activity in humans. *Clin Sci (Lond).* 1996;91:201-8.
 22. Karmakar CK, Gubbi J, Khandoker AH, Palaniswami M: Analyzing temporal variability of standard descriptors of Poincaré plots. *J Electrocardiol* 2010;43:719-24.
 23. Hayano J, Takahashi H, Toriyama T, Mukai S, Okada A, Sakata S, Yamada A, Ohte N, Kawahara H: Prognostic value of heart rate variability during long-term follow-up in chronic haemodialysis patients with end-stage renal disease. *Nephrol*

- Dial Transplant 1999;14:1480-8.
24. Aljadeff G, Gozal D, Schechtman VL, Burrell B, Harper RM, Ward SL: Heart rate variability in children with obstructive sleep apnea. *Sleep* 1997;20:151-7.
25. Muralikrishnan K, Balasubramanian K, Ali SM, Rao BV: Poincare plot of heart rate variability: an approach towards explaining the cardiovascular autonomic function in obesity. *Indian J Physiol Pharmacol* 2013;57:31-7.
26. Hutson JM, Mueller-Heubach E: Diagnosis and management of intrapartum reflex fetal heart rate changes. *Clin Perinatol* 1982;9:325-7.
27. Abrão KC, Francisco RP, Miyadahira S, Cicarelli DD, Zugaib M: Elevation of uterine basal tone and fetal heart rate abnormalities after labor analgesia: a randomized controlled trial. *Obstet Gynecol* 2009;113:41-7.
28. Downs HS, Morrison PH: The effects of spinal anesthesia on the fetal heart rate. *Calif Med* 1963;99:374-7.

3.2 Nonlinear Analysis of Fibrillatory Electrogram Similarity to Optimize the Detection of Complex Fractionated Electrograms During Persistent Atrial Fibrillation



3.2.1 INTRODUCTION

Atrial fibrillation (AF) is the most common type of tachyarrhythmia encountered in clinical practice.¹ Pulmonary vein isolation (PVI) has become the mainstream catheter ablation technique for AF.² For persistent AF, substrate modification with complex fractionated atrial electrogram (CFE) ablation is considered to be necessary in patients who have not responded to PVI.^{2,3} Recently, a randomized controlled trial demonstrated that termination of persistent AF by CFE ablation is not simply the result of atrial debulking. Ablating certain types of CFEs increases the cycle length of AF, suggesting that they were important in maintaining AF.⁴ Currently, the identification of CFEs is mostly based on cycle length-derived algorithms or a dominant frequency (DF) analysis.⁵⁻⁷ However, the data regarding the characteristics of the electrogram morphology and their consistency over time in the prediction of the efficacy of CFE ablation are still limited. We proposed that a temporal variation in the electrogram morphology was able to reflect the substrate nature and was helpful to localize critical regions. However, the fibrillation electrogram often exhibits the unpredictability and a waveform analysis based on a linear assumption of the signal only could give suboptimal results.⁸ We therefore tried to apply a nonlinear waveform analysis to study the morphological features of fibrillation electrograms. The aims of this study were: (1) to develop a novel nonlinear technique to identify the locally meaningful activations of fibrillation electrograms and quantify their waveform similarity; (2) to investigate the waveform similarity among the local activations of fibrillatory electrograms by the nonlinear method in both CFE and non-CFE atrial regions in comparison with other conventional linear parameters of fibrillatory electrograms; (3) to optimize the algorithm of targeting important CFEs based on the fibrillatory electrogram similarity quantified by our nonlinear method. The importance of the different types of CFEs was determined by procedural AF termination and long-term follow-up of freedom from atrial arrhythmias.



3.2.2 METHODS

Patient Characteristics

This study enrolled 100 symptomatic drug-refractory nonparoxysmal AF patients who received radiofrequency ablation guided by a NavX system (St. Jude Medical, Inc., St. Paul, MN, USA). The AF patients who had spontaneous termination of AF before ablation were excluded from this study.⁴

Electrophysiological Study

After acquiring the LA geometry, a 4-mm tip catheter was selected as the “roving” catheter for sequential contact mapping.⁹ The points in each region were similar in number and were nearly equally distributed.⁹

High-density mapping during AF performed in each patient was acquired and characterized by the linear analysis modalities and nonlinear analysis modalities. Linear analysis recording techniques were mostly based on a priori basis and time-dependent derivatives, including a frequency-domain analysis (DF and harmonic index [HI]) and time-domain analysis (fractionation interval [FI]). That is, frequency domain analyses commonly use a Fourier transform to reconstruct the raw signals with multiple continuous sinusoidal waves with fixed amplitudes and frequencies whereas the mean FI calculates the average length of the intervals between the CFE deflections. Both parameters are generated by linear operations. Regarding the frequency analysis, each intra-atrial recording was filtered with a second-order, zerophase Butterworth filter at 40–250 Hz.^{10,11} A second-order, zero-phase filter at 20 Hz was then applied to the absolute value of the resulting signal. The method of QRS-T subtraction was described previously.^{12,13} The final step of the process involved the frequency analysis. A fast Fourier transform (FFT) with a Hamming window was performed for each 6.82-second continuous segment from the multiple recording sites. Concerning the duration for the FFT analysis, a longer analysis interval (6.8 seconds; 1200 Hz, resolution 0.14 Hz) might have resulted in spectral noise, which could have interfered with the identification of the DF.¹¹ The ratio of the power of the DF and its harmonic peaks to the total power was defined as the HI, representing the organization and local temporal regularity of the AF.^{14,15}

The interval analysis was performed by using the builtin software of the NavX. The

CFE-mean (mean FI) was an interval-analysis algorithm that measured the average index of the fractionation at each site and in combination with 3-D mapping of the atrium, it could produce a color map representative of the CFE distribution in the atrium. Previously, we demonstrated that the continuous CFEs were defined by an averaged FI of ≤ 60 milliseconds over 5 seconds.¹² Variable CFEs were defined as having a mean FI between 60–120 milliseconds. The non-CFEs were defined as having a FI of >120 milliseconds.¹²

Nonlinear Waveform Analysis of Fibrillation Electrogram Similarities

Nonlinear analysis was performed by calculating bipolar repetitiveness from a continuous recording of 6 seconds from each of the intracardiac recordings (exported from the NavX mapping system). The step-by-step nonlinear analysis used to quantify the waveform similarity of the local fibrillation electrogram is demonstrated in Figures 1-3 and the details of the algorithm are described in the supplementary material.

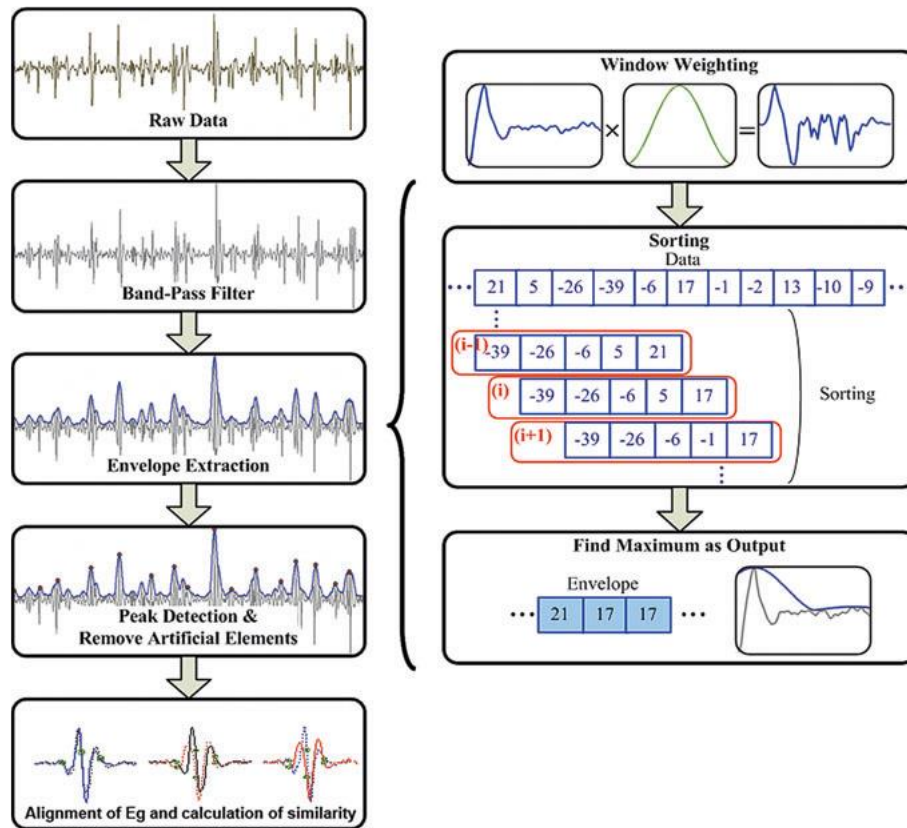


Figure 1. The left panel shows the flow chart of the nonlinear waveform analysis processing procedure and the right panel shows the schematic examples of the envelope function to detect the local activity waveform (LAW).

Briefly, first, the fibrillation electrogram was band-passed filtered for preprocessing

(40–250 Hz), and then the associated envelope was obtained by a proposed order-statistic filter which intensify the important activation of local electrograms.¹³ Second, to determine the critical components of the fibrillation electrogram, local activation waveforms (LAWs) were identified by the location where the peaks of the electrogram and envelope coincide. Third, the normalized electrograms within the LAWs could be regarded as the multidimensional vector; we used the nonlinear method to determine the functional distance between every vector (LAW) pair, as proposed by Faes et al.¹⁶ The percentage of LAWs pairs with functional distance below the threshold, indicating how many pairs of LAWs are similar, can be quantified as the similarity index (SI). It is worth noticing that the regularity, calculated by the conventional accumulation of each activated-wave deviation from the averaged template, could be serious degraded owing to the infrequent false detection of nonactivated waves. Meanwhile, this newly proposed algorithm (see Fig. 2) will minimize the influences of infrequent false detection and, therefore, is more robust than the conventional one.

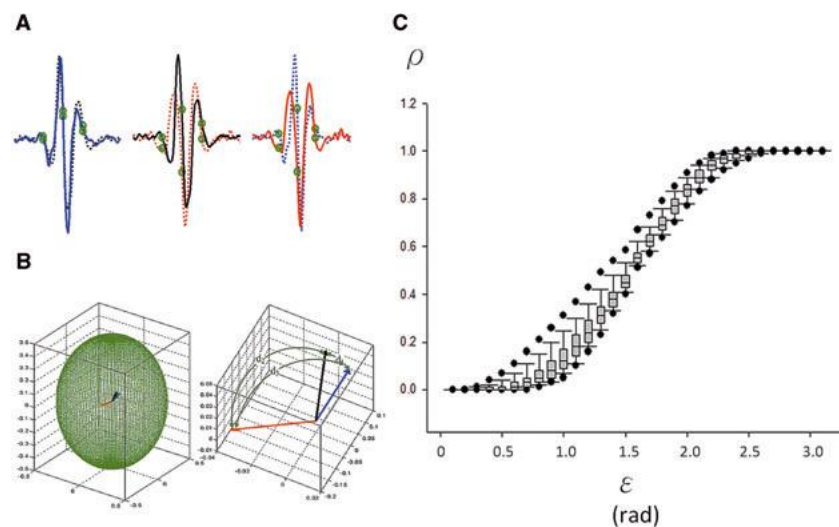


Figure 2. A 3-D example of the waveform comparison (A) and distance calculation (B) and finding an optimal threshold distance ϵ for the similarity index ρ (C). Panel (A) gives 3 waveform pair comparisons of LAWs, and the green circles indicate samples at 3 different time points in LAWs, and the sampled amplitude values of each waveform can be mapped to the magnitude in the x, y, and z directions, respectively. The left panel in (B) illustrates the mapping vectors corresponding to the waveforms in (A). Note that in these 3 paired LAWs, the sampled values of the LAWs were the closest between the red and black LAWs, which can be quantified by the functional distance between LAW pairs. The right panel in (B) gives a zoom-in picture, the radian between each vector pair is defined as the distance between each waveform pair, and ρ can be calculated from the ratio of the number of similar LAW pairs (distances of the pairs less than ϵ) to the total number of LAW pairs in the analyzed recording. (C) Shows the box-and-whisker plot of the average values of the ρ calculated from the total of

all the patients with atrial fibrillation as a function of the threshold distance ϵ . The error bars of the plot indicate the 10th and 90th percentile of ρ and the 2 black dots stand for the 5th and 95th percentile of ρ . The distribution was different for a ϵ ranging from 0.1 to 3.14 (ANOVA), with a maximal significance of $\epsilon = 1.1$.

Furthermore, 2 specific modifications from the previous method¹⁶ were implemented to diminish the interferences of far field contamination. The most crucial step of the regularity algorithm identification of LAWs from nonstationary background fibrillation was performed by a nonlinear strategy, an order-statistic filter. The envelope of the fibrillation electrogram can be constructed adaptively by local features of the electrograms by an order-statistic filter, and can, therefore, identify the nonlinear LAWs more accurately than the traditional linear low-pass filter (Fig. 3). Moreover, for the activated waves with very short wavelengths (e.g., sites of continuous CFAEs), we aligned the waveforms with their maximum peaks to improve the statistical regularities. In this study, continuous CFEs (mean FI ≤ 60 milliseconds in the LA and coronary sinus [CS]) were targeted, and the endpoint was procedural AF termination. We investigated the predictors of various signal characteristics of the CFEs on procedure termination and AF recurrence in a long-term follow-up.

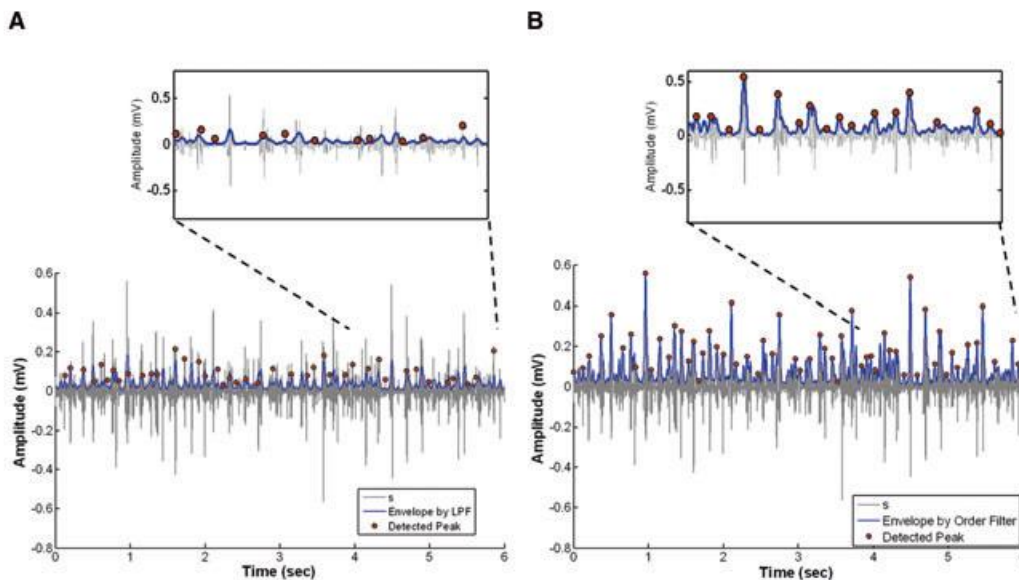
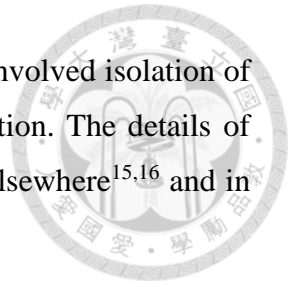


Figure 3. Performance comparison of the envelop generated from low-pass filter (A) and order-statistic filter (B) for a 6-second recording at a complex fractionated atrial electrogram site and both figures are zoomed in for the last 2 seconds. The order-statistic filter achieved a better performance for the LAW peak detection (red circle) related to the atrial activation waves.

Catheter Ablation

The stepwise procedure of the catheter ablation of persistent AF involved isolation of the PVs, a continuous CFAE ablation, and non-PV ectopy elimination. The details of the ablation procedure in nonparoxysmal AF have been described elsewhere^{15,16} and in the supplementary material.



Follow-Up of AF Recurrence

After discharge, the patients underwent follow-up (2 weeks after the catheter ablation, then every 1–3 months thereafter) at our cardiology clinic or with the referring physicians where routine ECGs were obtained during each follow-up, and antiarrhythmic drugs were prescribed for 8 weeks to prevent any early recurrence of AF. When the patients experienced symptoms suggestive of a tachycardia after the ablation, 24-hour Holter monitoring and/or cardiac event recording with a recording duration of 1 week were performed to define the cause of the clinical symptoms.⁴ The endpoint for the follow-up was clinically documented recurrence of any atrial arrhythmia.

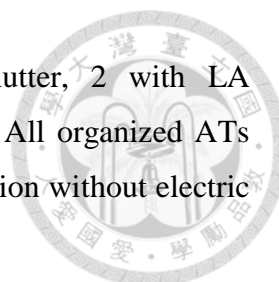
Statistical Analysis

All continuous data were presented as the mean value \pm standard deviation (SD). A chi-square test with Fisher's exact test was used for the categorical data. The means of continuous data of 2 groups were compared with the Student's t-test. Comparisons of more than 2 groups were performed with a one-way ANOVA. A Pair t-test was used for comparison of the substrate properties before and after PVI. Variables selected to be tested in the multivariate analysis were those with a P value < 0.2 in the univariate models. All statistical significances were set at a P < 0.05 .

3.2.3 RESULTS

Ablation Procedure

A total of 100 consecutive persistent AF patients received catheter ablation. In the step 1 ablation procedure, PVI could not terminate the AF in these 79 patients (79%). After PVI, substrate modification was performed targeting continuous CFEs in the LA and CS, and AF was terminated in 27 patients (39% of 69 patients, 10 patients received cardioversion before the CFE ablation). The procedural AF termination sites were located in the LA in 21 patients (78%), CS in 4 (15%), and RA in 2 (7%). After the CFE ablation, AF directly converted to sinus rhythm in 17 patients and to organized atrial



tachycardia (AT) in 7, including 3 with RA typical atrial flutter, 2 with LA roof-dependent reentry, and 2 with focal AT from the PV ostium. All organized ATs were mapped and responded to focal ablation and/or LA linear ablation without electric cardioversion.

In Table 1, patients with termination had a smaller LA, less hypertension, and heart failure history. These patients had a higher long-term single procedure success rate, and higher multiple procedure success rate, compared to the patients without termination.

Electrogram Characteristics of the CFEs Versus Non-CFEs

A total of 9,558 fibrillatory electrograms were analyzed in this study (139 ± 30 sites per patient in the LA). Table 2 shows the electrogram characteristics in the continuous CFE, noncontinuous CFE, and non-CFE sites. The electrogram similarity was higher in the continuous CFE compared to the noncontinuous CFE and non-CFE sites ($P < 0.05$), indicating less variability of the LAW in the continuous CFEs (Table 2).

TABLE 1
Baseline Characteristics

Variables	AF Termination	AF Nontermination	P Value
Age (year)	56 \pm 9.9	52 \pm 9.6	0.18
Male, n (%)	21 (78%)	36 (53%)	0.24
Hypertension, n (%)	7 (26%)	27 (64%)	0.004
Diabetes mellitus, n (%)	2 (7.4%)	7 (17%)	0.51
Hyperlipidemia, n (%)	5 (23%)	8 (29%)	0.75
Coronary artery disease, n (%)	3 (11%)	8 (19%)	0.14
Heart failure history, n (%)	1 (3.7%)	12 (29%)	0.024
Left atrial diameter (mm)	40 \pm 6.9	46 \pm 6.3	0.003
Left ventricular ejection fraction (%)	60 \pm 6.2	51 \pm 9.4	0.02
Sinus rhythm maintenance after a single procedure	24 (89%)	14 (33%)	<0.001
Sinus rhythm maintenance after multiple procedures	26 (96%)	23 (55%)	0.001

TABLE 2
Summary of the Signal Analysis of the Continuous CFE Sites, Noncontinuous CFE Sites, and Non-CFE Sites in All Patients

Location	DF (Hz)	HI	FI (milliseconds)	Similarity Index (ρ)
Continuous CFE	7.2 \pm 1.37*	0.38 \pm 0.041	52 \pm 5.5*	0.54 \pm 0.093*
Noncontinuous CFE	6.5 \pm 1.48 ⁺	0.39 \pm 0.044	82 \pm 17 ⁺	0.50 \pm 0.102 ⁺
Non-CFE sites	6.1 \pm 1.40	0.38 \pm 0.050	216 \pm 199	0.45 \pm 0.123

CFE = complex fractionated atrial electrogram; DF = dominant frequency; FI = mean fractionation interval over 6 seconds; HI = harmonic index.

* $P < 0.05$ when compared to the noncontinuous and non-CFE sites; ⁺ $P < 0.05$ when compared to the non-CFE sites.



Electrogram Characteristics in Patients Who Did or Did Not Respond to CFE

Ablation

Substrate mapping of the global atria

Comparison of the electrogram characteristics of the entire LA in the patients who did and did not respond to CFE ablation in terms of procedural AF termination and long-term AF recurrence is shown in Figure 4. Patients with atrial substrate characteristics harboring rapid activity and more fractionated electrograms were less likely to respond to CFE ablation, as indicated by a higher DF ($P < 0.05$), and higher proportion of CFEs in the LA ($P < 0.01$).

Correlation of ablation outcome and electrogram characteristics

In Table 3, the electrogram characteristics of the targeted CFEs (continuous CFEs: 17% of LA) did not differ based on the linear analysis modalities (DF, HI, and FI) between the patients who responded and did not respond to the CFE ablation. In contrast, the averaged SI of the targeted CFEs was higher in patients with successful procedural AF termination and in AF recurrence-free patients. Such a disparity in the similarity was not observed in the noncontinuous CFEs (0.51 ± 0.09 vs 0.51 ± 0.11 ; $P = \text{NS}$) and non-CFEs (0.41 ± 0.13 vs 0.44 ± 0.11 ; $P = \text{NS}$) sites in the patients with and without termination, respectively.

Characteristics of the Procedural AF Termination Sites

The raw electrograms and CFE deflections (Fig. 5A) as well as their overlapped normalized LAW electrograms and the top 6 LAWs with closest functional distances (Fig. 5B) were shown based on the different levels of similarity. In addition to high morphological waveform similarity, the CFE deflections were temporally well aligned in high similarity areas. Figure 6A shows an example of procedural AF termination in the posterolateral LA, where a high level of SI was compatible with the maximal CFEs. In contrast, in Figure 6B, ablation of the maximal CFE in the lateral mitral annulus and LA septum could not terminate AF. A subsequent roofline ablation (with a mean FI of 76 milliseconds; $\text{SI} = 0.81$) terminated AF without any AF recurrence during the long-term follow-up.

The Optimal Detection Algorithm for CFEs

Within all the CFE regions, a univariate analysis showed that shorter mean FI and higher SI were both associated with procedural AF termination. The DF value, HI value, and electrogram voltage did not correlate with the termination ($P > 0.05$). A multivariate regression analysis showed that only a higher SI (≥ 0.57 ; odd ratio [OR] = 4.9; 95% CI = 1.33–18.0; $P = 0.017$) predicted procedural AF termination. Sites with a shorter mean FI did not predict procedural termination (< 70 milliseconds; OR = 1.69; 95% CI = 0.61–4.67; $P = 0.31$).

3.2.4 DISCUSSION

Main Findings

This study demonstrated that patients with a high level of electrogram morphology similarity at the CFEs sites, quantified by a novel nonlinear technique, were more likely to respond to substrate modification by targeting continuous CFEs. Regional disparities in the electrogram characteristics of patients with persistent AF between the important CFE/CFEs and bystander CFEs were difficult to identify by the interval analysis, DF value, and temporal variation in the DF peak. Targeting sites with a high level of electrogram similarity in the fractionated electrograms in the LA was associated with procedural AF termination and a better long-term outcome after the first ablation procedure.

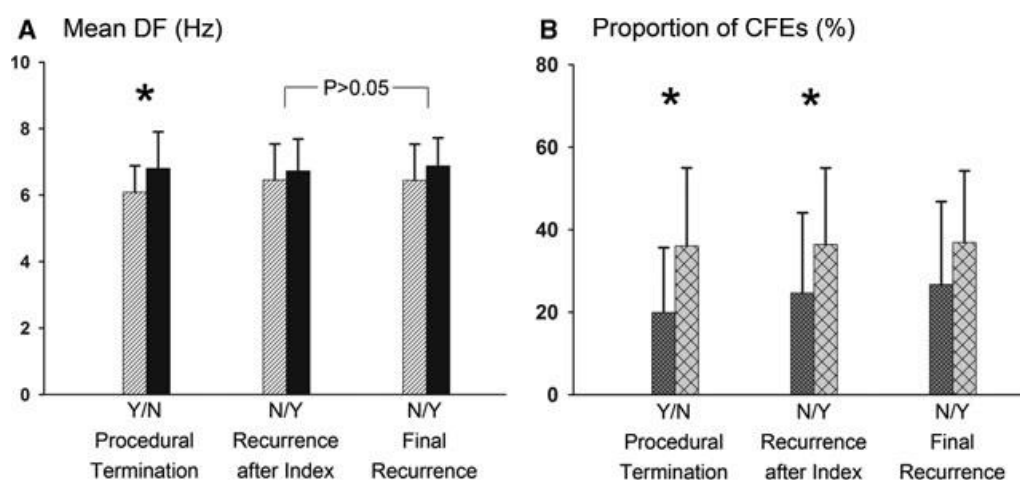


Figure 4. Summary of the signal analysis, including the mean dominant frequency (Panel A) and proportion of the continuous CFEs (Panel B) of the left atrium for predicting AF procedural termination, recurrence after the first ablation procedure, and recurrence after the final procedure.

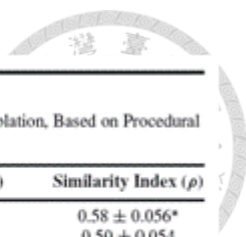


TABLE 3
Summary of the Signal Analysis of the Continuous CFE Sites in the LA in Patients Who Did and Did Not Respond to CFE Ablation, Based on Procedural Termination and AF Recurrence after Ablation

		DF (Hz)	HI	FI (milliseconds)	Similarity Index (ρ)
AF termination	Patients with termination	6.4 ± 1.34	0.40 ± 0.014	53 ± 5.0	0.58 ± 0.056*
	Patients without termination	7.0 ± 0.74	0.39 ± 0.025	53 ± 4.2	0.50 ± 0.054
AF recurrence	No AF recurrence after a single procedure	6.8 ± 1.56	0.39 ± 0.017	53 ± 4.5	0.57 ± 0.055*
	AF recurrence after single a procedure	6.8 ± 0.95	0.39 ± 0.020	53 ± 4.6	0.50 ± 0.050

*P < 0.01 when compared to sites without termination, and recurrence after the procedure.

Fractionated Electrograms by the Time-Domain Signals

Since the work of Nademanee et al., ablation of CFEs has become a standard component for substrate modification of persistent AF. The efficacy of adjunctive CFE ablation in addition to circumferential PVI has been confirmed in patients with persistent AF, irrespective of the definition of a CFE.^{2,3} Automatic algorithms for 3-D mapping systems have provided a rigorous quantitative analysis enabling the identification of the CFEs and continuous CFEs as well as the stability of the CFE distribution over time. Different definitions of CFE may partly explain the different results of catheter ablation. Previous studies demonstrated that certain types of CFEs could be the AF drivers, and some types may represent passive wavefront collision.^{4,17} Simply based on time-domain electrograms, it is difficult to distinguish which type of CFEs may play an active role in persistent AF. Previously, ablating sites with a greater percentage of continuous activity was associated with slowing the AF or procedural AF termination in patients with chronic AF.¹⁸ Several studies examined the stability of fractionated electrogram, and demonstrated that the consistency of the interval was higher in the CFEs sites as compared to the non-CFE sites.^{12,19} Sander's laboratory and Chen's laboratory demonstrated that the maximal fractionated sites were observed at or adjacent to these high DF sites.²⁰ Recently, Narayan classified fractionated electrograms into different types, and a small proportion of CFE sites exhibited rapid, discrete, and organized recordings consistent with an AF driver.²¹ Therefore, the of the CFE that maintains AF should be continuous, fast, and stable over time.

Previously, there was a paucity of data regarding the consistency of consecutive fibrillatory electrogram morphologies, and it is rarely applied in clinical mapping.²² In this study, we applied the nonlinear envelope function to magnify the detection of each of the fibrillatory electrograms (LAW) and a comparison of the consecutive LAWs was performed. The measurement was based on the assumption that the repetitive waveforms of similar electrogram morphologies were near the potential AF maintainers. Consistent

wavefront dynamics and activation patterns were emanating from the AF sources and caused repetitive and similar electrogram morphologies. This study demonstrated that a higher level of the electrogram SI at the sites with continuous CFEs was more likely to respond to substrate modification and it could provide an alternative mapping tool to guide substrate modification.

Definition of Fractionated Electrograms by Spectral Morphology

The fast Fourier analysis has been used to estimate the fibrillation cycle length by the DF and the irregularity of the fibrillation electrograms.²³ The DF value represents the average fibrillation cycle lengths during AF. However, the regional DF value may not be reliable because of the limited gradient of the regional DF in patients with long-lasting persistent AF.^{6,20,24-27} Investigators have also applied the organization or HI to quantify the degree of fractionation.²⁸ These factors may represent the irregularity of the cycle length, fractionation electrograms, or even background noise. In fact, the indices of the spectral morphology, i.e., the DF and HI, may be easily compromised by the presence of chaotic signals. In seemingly chaotic fibrillatory signals, the DF peaks are less prominent, and might not accurately reflect the local fibrillation cycle length.²⁹ In this study, we found no disparities in the degree of organization of AF between the culprit CFEs and bystander CFEs when quantifying the organization of the fibrillation, the HI, an indicator of the complexity of the fibrillation electrogram based on frequency spectra. This result indicated that it is difficult to optimize the CFE detection by comparing the indices derived from the spectral morphology.

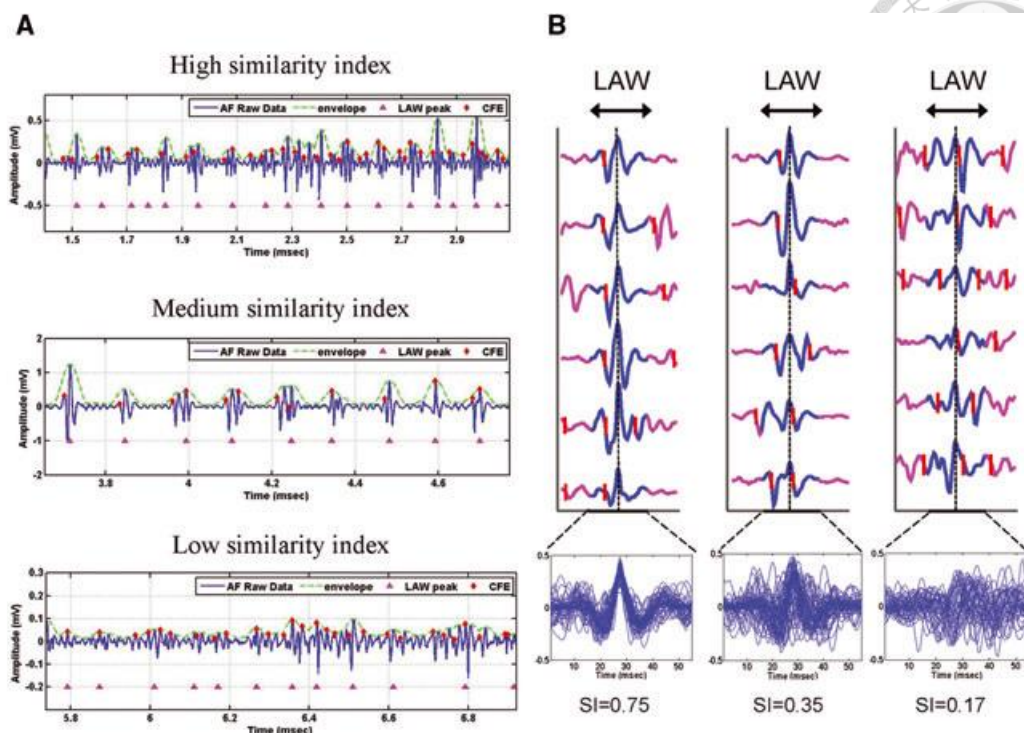
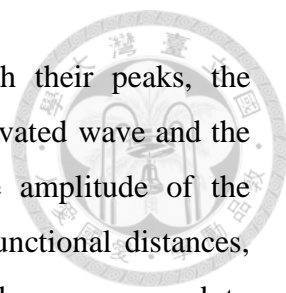


Figure 5. Analysis of the electrogram similarity with different types of continuous complex fractionated electrograms (CFE). Typical bipolar fractionated electrograms including rapid activity and continuous electrograms with high, medium, and low similarity (Panel A) and the top 6 LAWs with the closest functional distances of the continuous CFE sites with a different similarity (Panel B) are demonstrated. In panel A, the envelope function of the filtered data (green dotted line), centers of the LAWs (magenta triangle), and start points of the CFE deflections (red triangle) are shown. Each LAW consists of multiple deflections and some of those might be CFE deflections. The upper 3 tracings in panel B, from left to right, demonstrate the top 6 LAWs with the closest functional distances at high, medium, and low similarity sites, and the bottom tracings are the normalized electrograms of all the LAWs overlapping with their center peaks and corresponding similarity index.

Advantage of a Similarity Analysis by a Nonlinear Waveform Analysis

The waveform similarity of the time-domain fractionated electrograms during AF was complex and difficult to analyze because of the variable amplitude and electrogram morphology. Especially for bipolar electrograms, the deflections could have either positive, negative or polyphasic polarities. In this study, we applied the nonlinear envelope function to intensify the detection of the electrogram peaks over the background interference, rather than depicting the peak deflections. After the important peaks of the fibrillatory electrograms were identified, the segments of the LAWs could be derived with a predefined window size. Instead of using one single deflection, multiple deflections were found within the window and could be covered when we



calculated the SI. Moreover, after alignment of the LAWs with their peaks, the amplitude of each LAW was normalized by the SD of the local activated wave and the value of the SI was, therefore, irrelevant to the change in the amplitude of the deflections among different identified windows. In addition, the functional distances, obtained from each of 2 waveforms within the segmented window, were used to calculate the SI rather than the summation of the deviation from the averaging template as a linear calculation.

Morphological Features of CFEs with a High SI

By the aforementioned algorithm, the morphological change in regard to the temporal distribution of the different types of deflections either positive or negative, total duration of the discrete electrograms, and intervals between consecutive deflections within the segmented windows were all contributed to the calculation of the SI. With the proposed nonlinear analysis for the similarity between the LAWs, the culprit CFEs were identified with a high degree of repetitive waveform morphology patterns that coincided with the same sequence of the CFE deflections. For example, the trace with a higher SI presented a more consistent interval between the CFE deflections and LAW alignment (Fig. 5). Accordingly, the degree of organization of the AF was quantified by the temporal distribution of the fibrillation electrogram morphology complexity, irrespective of the distribution of the fibrillation cycle length. This provides an alternative mapping tool to guide substrate modification.

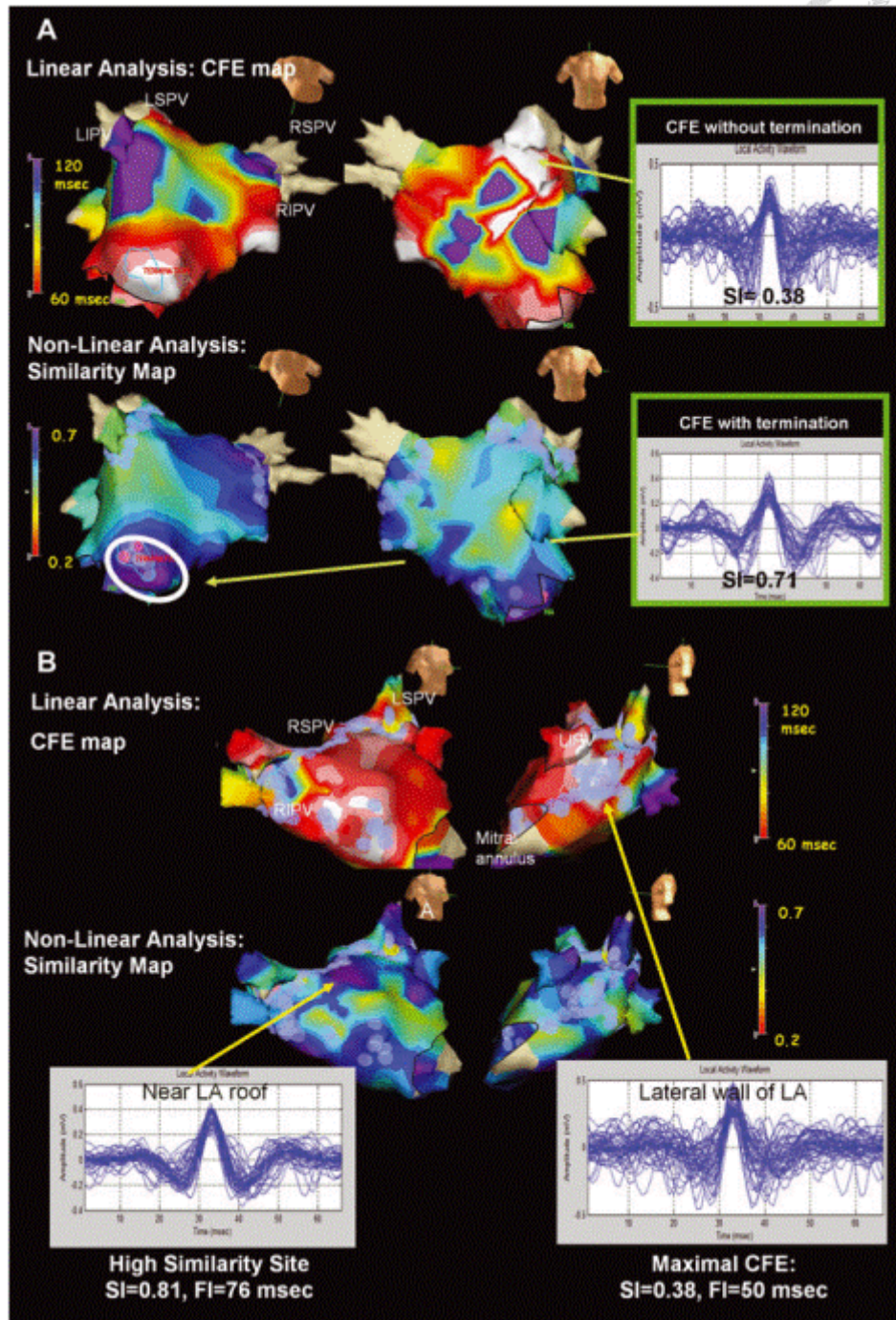
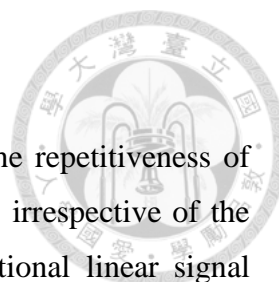


Figure 6. Examples of a 3-D similarity map and fractionation map in a patient with (Panel A) and a patient without (Panel B) procedural AF termination. In panel A, the maximal fractionated sites were identified with the high similarity index in the lateral mitral isthmus region. The similarity index locally was 0.71, whereas the similarity index of the CFEs in the anterior wall was 0.38. In panel B, the maximal CFE was not associated with the high similarity index. The highest similarity near the border of the continuous CFEs was identified in the roof region. In this patient, ablation in the roof region terminated the AF with final sinus rhythm maintenance during the long-term follow-up.



3.2.4 CONCLUSIONS

This study introduced a novel nonlinear technique to quantify the repetitiveness of consecutive fibrillation electrograms in patients with persistent AF, irrespective of the intervaldependent variables. Within the continuous CFEs, conventional linear signal analysis could not differentiate the termination sites from nontermination sites. Targeting CFE sites in the presence of a high level of electrogram similarity of the fractionated electrograms in the LA was correlated with the procedural AF termination and freedom from AF recurrence after the index procedure. This study suggested that sites with a high level of fibrillation electrogram similarity at the CFEs are important for AF maintenance.

Study Limitations

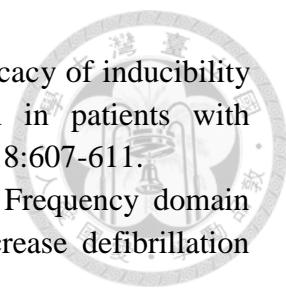
First, the high SI sites outside the continuous CFEs were not targeted. However, this study demonstrated that most of the high SI sites were located within the continuous CFEs.

Second, the CFE ablation was not based on the SI. However, in this study, the continuous CFEs (mostly the highest similarity sites) were targeted first and procedural AF termination was the endpoint of procedure. After procedural termination, sites with lesser degree of continuous CFEs were not targeted. A recent study demonstrated that the proportion of the lesions causing termination was not affected by the order of ablating the targeted CFE sites.⁴

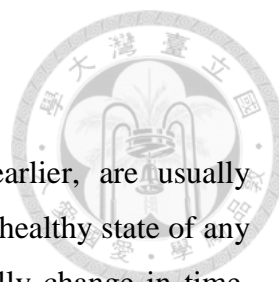


REFERENCES

1. Nattel S: New ideas about atrial fibrillation 50 years on. *Nature* 2002;10;415:219-226.
2. Hayward RM, Upadhyay GA, Mela T, Ellinor PT, Barrett CD, Heist EK, Verma A, Choudhry NK, Singh JP: Pulmonary vein isolation with complex fractionated atrial electrogram ablation for paroxysmal and nonparoxysmal atrial fibrillation: A meta-analysis. *Heart Rhythm* 2011;8:994-1000.
3. Calkins H, Brugada J, Packer DL, Cappato R, Chen SA, Crijns HJ, Damiano RJ Jr, Davies DW, Haines DE, Haissaguerre M, Iesaka Y, Jackman W, Jais P, Kottkamp H, Kuck KH, Lindsay BD, Marchlinski FE, McCarthy PM, Mont JL, Morady F, Nademanee K, Natale A, Pappone C, Prystowsky E, Raviele A, Ruskin JN, Shemin RJ: HRS/EHRA/ECAS expert Consensus Statement on catheter and surgical ablation of atrial fibrillation: Recommendations for personnel, policy, procedures and follow-up. A report of the Heart Rhythm Society (HRS) Task Force on catheter and surgical ablation of atrial fibrillation. *Heart Rhythm* 2007;4:816-861.
4. Hunter RJ, Diab I, Tayebjee M, Richmond L, Sporton S, Earley MJ, Schilling RJ: Characterization of fractionated atrial electrograms critical for maintenance of atrial fibrillation: A randomized, controlled trial of ablation strategies (the CFAE AF trial). *Circ Arrhythm Electrophysiol* 2011;4:622-629.
5. Atenza F, Almendral J, Jalife J, Zlochiver S, Ploutz-Snyder R, Torrecilla EG, Arenal A, Kalifa J, Fernández-Avilés F, Berenfeld O: Real-time dominant frequency mapping and ablation of dominant frequency sites in atrial fibrillation with left-to-right frequency gradients predicts long-term maintenance of sinus rhythm. *Heart Rhythm* 2009;6:33-40.
6. Verma A, Novak P, Macle L, Whaley B, Beardsall M, Wulffhart Z, Khaykin Y: A prospective, multicenter evaluation of ablating complex fractionated electrograms (CFEs) during atrial fibrillation (AF) identified by an automated mapping algorithm: Acute effects on AF and efficacy as an adjuvant strategy. *Heart Rhythm* 2008;5:198-205.
7. Nademanee K, McKenzie J, Kosar E, Schwab M, Sunsaneewitayakul B, Vasavakul T, Khunnawat C, Ngarmukos T: A new approach for catheter ablation of atrial fibrillation: Mapping of the electrophysiologic substrate. *J Am Coll Cardiol* 2004;43:2044-2053.
8. Alcaraz R, Rieta JJ: Non-linear organization analysis of paroxysmal atrial fibrillation. *Conf Proc IEEE Eng Med Biol Soc* 2007;2007:1957-1960.
9. Lo LW, Tai CT, Lin YJ, Chang SL, Wongcharoen W, Chang SH, Hsieh MH, Tuan TC, Udyavar AR, Chen YJ, Tsao HM, Chen SA: Progressive remodeling of the atrial substrate—a novel finding from consecutive voltage mapping in patients with recurrence of atrial fibrillation after catheter ablation. *J Cardiovasc Electrophysiol* 2007;18:258-265.
10. Chang SL, Tai CT, Lin YJ, Wongcharoen W, Lo LW, Tuan TC, Udyavar AR, Chang

- 
- SH, Tsao HM, Hsieh MH, Hu YF, Chen YJ, Chen SA: The efficacy of inducibility and circumferential ablation with pulmonary vein isolation in patients with paroxysmal atrial fibrillation. *J Cardiovasc Electrophysiol* 2007;18:607-611.
11. Everett TH, Kok LC, Vaughn RH, Moorman JR, Haines DE: Frequency domain algorithm for quantifying atrial fibrillation organization to increase defibrillation efficacy. *IEEE Trans Biomed Eng* 2001;48:969-978.
 12. Lin YJ, Tai CT, Kao T, Chang SL, Wongcharoen W, Lo LW, Tuan TC, Udyavar AR, Chen YJ, Higa S, Ueng KC, Chen SA: Consistency of complex fractionated atrial electrograms during atrial fibrillation. *Heart Rhythm* 2008;5:406-412.
 13. Cheng F, Venetsanopoulos AN: An adaptive morphological filter for image processing. *IEEE Trans Image Process* 1992;1:533-539.
 14. Lin YJ, Tai CT, Kao T, Chang SL, Lo LW, Tuan TC, Udyavar AR, Wongcharoen W, Hu YF, Tso HW, Tsai WC, Chang CJ, Ueng KC, Higa S, Chen SA: Spatiotemporal organization of the left atrial substrate after circumferential pulmonary vein isolation of atrial fibrillation. *Circ Arrhythm Electrophysiol* 2009;2:233-241.
 15. Lin YJ, Tai CT, Chang SL, Lo LW, Tuan TC, Wongcharoen W, Udyavar AR, Hu YF, Chang CJ, Tsai WC, Kao T, Higa S, Chen SA: Efficacy of additional ablation of complex fractionated atrial electrograms for catheter ablation of nonparoxysmal atrial fibrillation. *J Cardiovasc Electrophysiol* 2009;20:607-615.
 16. Faes L, Nollo G, Antolini R, Gaita F, Ravelli F: A method for quantifying atrial fibrillation organization based on wave-morphology similarity. *IEEE Trans Biomed Eng* 2002;49:1504-1513.
 17. Lo LW, Higa S, Lin YJ, Chang SL, Tuan TC, Hu YF, Tsai WC, Tsao HM, Tai CT, Ishigaki S, Oyakawa A, Maeda M, Suenari K, Chen SA: The novel electrophysiology of complex fractionated atrial electrograms: Insight from noncontact unipolar electrograms. *J Cardiovasc Electrophysiol* 2010;21:640-648.
 18. Takahashi Y, O'Neill MD, Hocini M, Dubois R, Matsuo S, Knecht S, Mahapatra S, Lim KT, Jaïs P, Jonsson A, Sacher F, Sanders P, Rostock T, Bordachar P, Clémenty J, Klein GJ, Haïssaguerre M: Characterization of electrograms associated with termination of chronic atrial fibrillation by catheter ablation. *J Am Coll Cardiol* 2008;51:1003-1010.
 19. Verma A, Wulffhart Z, Beardsall M, Whaley B, Hill C, Khaykin Y: Spatial and temporal stability of complex fractionated electrograms in patients with persistent atrial fibrillation over longer time periods: Relationship to local electrogram cycle length. *Heart Rhythm* 2008;5:1127-1133.
 20. Stiles MK, Brooks AG, Kuklik P, John B, Dimitri H, Lau DH, Wilson L, Dhar S, Roberts-Thomson RL, Mackenzie L, Young GD, Sanders P: High-density mapping of atrial fibrillation in humans: Relationship between high-frequency activation and electrogram fractionation. *J Cardiovasc Electrophysiol* 2008;19:1245-1253.
 21. Narayan SM, Wright M, Derval N, Jadidi A, Forclaz A, Nault I, Miyazaki S, Sacher F, Bordachar P, Clémenty J, Jaïs P, Haïssaguerre M, Hocini M: Classifying

- fractionated electrograms in human atrial fibrillation using monophasic action potentials and activation mapping: Evidence for localized drivers, rate acceleration, and nonlocal signal etiologies. *Heart Rhythm* 2011;8:244-253.
22. Chang SH, Ulfarsson M, Chugh A, Yoshida K, Jongnarangsin K, Crawford T, Good E, Pelosi F Jr, Bogun F, Morady F, Oral H: Time- and frequency-domain characteristics of atrial electrograms during sinus rhythm and atrial fibrillation. *J Cardiovasc Electrophysiol* 2011;22:851-857.
23. Kalifa J, Tanaka K, Zaitsev AV, Warren M, Vaidyanathan R, Auerbach D, Pandit S, Vikstrom KL, Ploutz-Snyder R, Talkachou A, Atenza F, Guiraudon G, Jalife J, Berenfeld O: Mechanisms of wave fractionation at boundaries of high-frequency excitation in the posterior left atrium of the isolated sheep heart during atrial fibrillation. *Circulation* 2006;113:626-633.
24. Lin YJ, Tsao HM, Chang SL, Lo LW, Hu YF, Chang CJ, Tsai WC, Suenari K, Huang SY, Chang HY, Wu TJ, Chen SA: The role of high dominant frequency sites in non-paroxysmal AF patients: Insights from high-density frequency and fractionation mapping. *Heart Rhythm* 2010;7:1255-1262.
25. Kester W: *Mixed-Signal and DSP Design Techniques*. Burlington, MA: Elsevier Science 2003; pp. 6.1-6.31.
26. Pallav P, Gan TH, Hutchins DA: Elliptical Tukey chirp signal for high-resolution, air-coupled ultrasonic imaging. *IEEE Trans Ultrason Ferroelectr Freq Control* 2007;54:1530-1540.
27. Ciaccio EJ, Biviano AB, Whang W, Gambhir A, Garan H. Spectral profiles of complex fractionated atrial electrograms are different in longstanding and acute onset atrial fibrillation atrial electrogram spectra. *J Cardiovasc Electrophysiol* 2012;23:971-979.
28. Everett TH, Kok LC, Vaughn RH, Moorman JR, Haines DE: Frequency domain algorithm for quantifying atrial fibrillation organization to increase defibrillation efficacy. *IEEE Trans Biomed Eng* 2001;48:969-978.
29. Ng J, Kadish AH, Goldberger JJ: Technical considerations for dominant frequency analysis. *J Cardiovasc Electrophysiol* 2007;18:757-764.



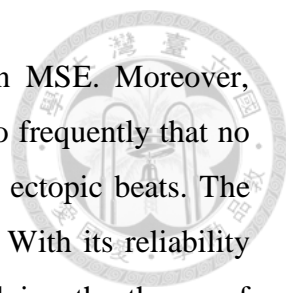
Chapter 4 Conclusion

Physiological data, from simple to complex, as mentioned earlier, are usually considered as the results of a running dynamic systems. The normal healthy state of any living system is in homeostasis, which is not static, but dynamically change in time, which exhibits high degree of complexity and highly orders. For biomedical signal processing, such complex systems is difficult to deal with, and hard to be described through limited clinical data. In this point, complex theory has been used, many nonlinear methods were then proposed in recent years, trying to describe and identify such complex phenomena on limited data. Base on these, this dissertation proposed several robust methods on quantization the multi-scale correlation and attracting orbits, try to extend the usage of nonlinear methodology and fulfill certain requirements.

Quantization of Multi-scale correlation

The multi-scale correlation on reconstructed phase space can quantify the complexity of a time series, however, the coarse-graining steps will result in less number of point in larger scale for reliable calculation. By rearrange the coarse-graining steps, the data points on large scale can be extended and hence increase the reliability. The cost for this would be the larger volume of computation. The results shows, by utilize the novel sMSE approach for PWV signal analysis, the time for data acquisition can be substantially reduced from 30 minutes to 10 minutes with remarkable preservation of sensitivity in differentiating among the healthy, aged, and diabetic populations compared with the conventional MSE method.

On the other hand, sample-entropy based calculation of correlation need a criteria for neighborhood which is easy to be effected by extreme value of outliers, as well as the coarse-graining steps are easy to be interfered by frequency happen outliers. Therefore, all previous complexity analyses require heartbeat signals without outliers or ectopic beats. Removing outliers or ectopic beats is not trivial, not only requiring specific expertise in ECG waveforms but also being very time-consuming. However, how the automatic filtering affects complexity measures is not known. In addition, the procedure works well in the signals with the occasional and isolated ectopic beats but may not be applicable in the data with numerous and often continuous ectopic beats as occurred in ECG data of ECMO patients. By utilize the symbolic dynamics method and replace the mean with median on the coarse-graining steps, the results demonstrated the recursive



automatic filtering only slightly attenuate the effect of outliers in MSE. Moreover, ectopic beats in certain patients such as the ECMO patients occur so frequently that no continuous heartbeat recordings can be obtained after removing all ectopic beats. The proposed MSSE was specially designed to resolve these problems. With its reliability and high resilience to outliers, the method gives the hope of applying the theory of complexity in clinical practice. Further validation of the method using a large sample size is warranted.

Quantification of Attracting Orbit

The attracting orbits reflect the real dynamics of a system, but the underlying rules are not easy to figure out. The Poincaré plot provides basic statistic information of cycle length which is important for HRV, however, need a method to identify each cycle at first. For the continuous monitoring FHR through HRV during CS, extracting from the maternal abdominal ECG remains a challenge since the electrodes cannot be placed properly. Moreover, the CS procedure would introduce large motion artifacts and myopotential interference which are difficult to deal with by using traditional methods. The proposed algorithms successfully identify each cycle of heart beat and demonstrate that abnormal FHR during spinal or epidural anesthesia are primarily the results of uterine hypertonus and maternal hypotension. The FHR was significantly increased but remained within the normal range, which might be attributed to vasodilatation caused by spinal anesthesia. The effective data are difficult to obtain because of the high possibility of contamination and interference during the delivery. As a result, the study population was small which need a larger population study in the future that could validate the meaning of the derived parameters.

On the other hand, identify the periodic orbit cycle in very complex dynamics system, such as determine the LAWs of the fibrillation electrogram in AF patient, is hard and crucial. Through the proposed nonlinear method, the LAWs as well as each periodic cycle were identified. Moreover, through the correlations of each identified orbits, the percentage of LAWs pairs indicating how many pairs of orbits are similar, can be quantified as the similarity index (SI). It is worth noticing that the regularity, calculated by the conventional accumulation of each activated-wave deviation from the averaged template, could not differentiate the termination sites from nontermination sites. This study also suggested that sites with a high level of fibrillation electrogram similarity at the CFEs are important for AF maintenance.